

# Age and origin of coeval TTG, I- and S-type granites in the Famatinian belt of NW Argentina

R. J. Pankhurst, C. W. Rapela and C. M. Fanning

**ABSTRACT** Three granitoid types are recognised in the Famatinian magmatic belt of NW Argentina, based on lithology and new geochemical data: (a) a minor trondhjemite-tonalite-granodiorite (TTG) group, (b) a metaluminous I-type gabbro-monzogranite suite, and (c) S-type granites. The latter occur as small cordieritic intrusions associated with I-type granodiorites and as abundant cordierite-bearing facies in large batholithic masses. Twelve new SHRIMP U–Pb zircon ages establish the contemporaneity of all three types in Early Ordovician times (mainly 470–490 Ma ago). Sr- and Nd-isotopic data suggest that, apart from some TTG plutons of asthenospheric origin, the remaining magmas were derived from a Proterozoic crust–lithospheric mantle section. Trace element modelling suggests that the TTG originated by variable melting of a depleted gabbroid source at 10–12 kbar, and the I-type tonalite–granodiorite suite by melting of a more enriched lithospheric source at c. 5 kbar. The voluminous intermediate and acidic I-types involved hybridisation with lower and middle crustal melts. The highly peraluminous S-type granites have isotopic and inherited zircon patterns similar to those of Cambrian supracrustal metasedimentary rocks deposited in the Pampean cycle, and were derived from them by local anatexis. Other major components of the S-type batholiths involved melting of deep crust and mixing with the I-type magmas, leading to an isotopic and geochemical continuum.

**KEY WORDS:** anatexis, geochemistry, Gondwana margin, modelling, palaeozoic, U–Pb geochronology, zircon

The exposed metamorphic and igneous basement of the Sierras Pampeanas developed on the western margin of Gondwana, through Cambrian accretion of the Pampean terrane, followed by the Late Ordovician/Silurian accretion of the Precordillera (Laurentian) terrane to the W (Fig. 1). The granitoids of the region were assigned to three main groups by Rapela *et al.* (1990, 1992) on the basis of K–Ar and Rb–Sr geochronological data. G1 consists of small dioritic and gabbroic bodies with Late Precambrian to Cambrian ages, ascribed to the Pampean cycle. G2 includes larger bodies and batholiths of a much broader compositional spectrum that constitute the Famatinian mobile belt, the subject of this paper—they display both syn-kinematic and post-kinematic styles with respect to Pampean deformation. G3 is a group of evolved, alkaline post-tectonic granitoids, apparently of Devonian–Carboniferous age.

Some Famatinian granites intrude Lower Ordovician sedimentary and volcanic rocks. In a recent summary of the geology of the Sierra de Famatina (note that place names are represented by letters in Fig. 1, see caption), Aceñolaza *et al.* (1996) ascribed the major plutonic activity to the Middle Ordovician–Silurian interval (460–410 Ma), as did Rapela *et al.* (1992). However, in the Puna, W of Salta, Lork & Bahlburg (1993) found consistent U–Pb monazite ages of 467–476 Ma for granites that may be a northern extension of the Famatinian belt. More recently, Pankhurst *et al.* (1998) published conventional and microprobe U–Pb zircon ages from the southern Sierras Pampeanas indicating major emplacement of I-type granodiorite suites from  $490 \pm 5$  Ma, although smaller bodies of monzogranite gave Rb–Sr ages ranging from 470 to 450 Ma. These data suggest that the Famatinian magmatic arc is predominantly of Early–Middle Ordovician age.

In this paper we present new U–Pb zircon data and geochemistry for Sierras Pampeanas granitoids, including the major batholiths of the Famatina belt. We show that three distinct types (I-type, S-type and TTG) can be distinguished

petrologically, geochemically and spatially, but that all were essentially contemporaneous, within the Tremadoc–Llanvirn interval. Geochemical modelling shows that they represent different levels of melting within the pre-Famatinian crust and coupled lithospheric mantle.



## 1. The granites of the Famatinian magmatic arc: lithology and spatial distribution

### 1.1. Tonalite–trondhjemite–granodiorite

The TTG group occurs as small to medium-sized plutons, only in the Pampean foreland region. Examples were first described in the Sierra de Cachi, in the northern Sierras Pampeanas (Fig. 1) by Galliski & Miller (1989) and Galliski *et al.* (1990), and dated as Ordovician by Lork *et al.* (1991). Similar bodies in the Sierras de Córdoba (Có in Fig. 1) have recently been assigned to the same episode; they post-date the main S2 structure of the country gneisses and migmatites, which originated in the Early-to-Middle Cambrian Pampean metamorphism (Rapela *et al.* 1998). The igneous fabrics are generally overprinted by S3 brittle deformation, producing fracture cleavage and kink structures in the micas (Caffe & Baldo 1994; Martino *et al.* 1995; Pérez *et al.* 1996). Abundant modal quartz (>27%) and plagioclase (>40%), scarce K-feldspar (0–4.5%) and mafic minerals (<10%) are characteristic of the tonalite–trondhjemite bodies along the eastern side of the Sierras de Córdoba; apatite, zircon, epidote and monazite are ubiquitous. Using the normative CIPW classification, compositions straddle the trondhjemite and tonalite fields (Fig. 2), and all contain biotite (3–8%) and muscovite (1–12%). High-Na granodiorite plutons in which a biotite–muscovite facies predominates crop out in the northwestern sector of the Sierras de Córdoba (Gomez & Lira 1998), and are also considered to belong to the TTG group.

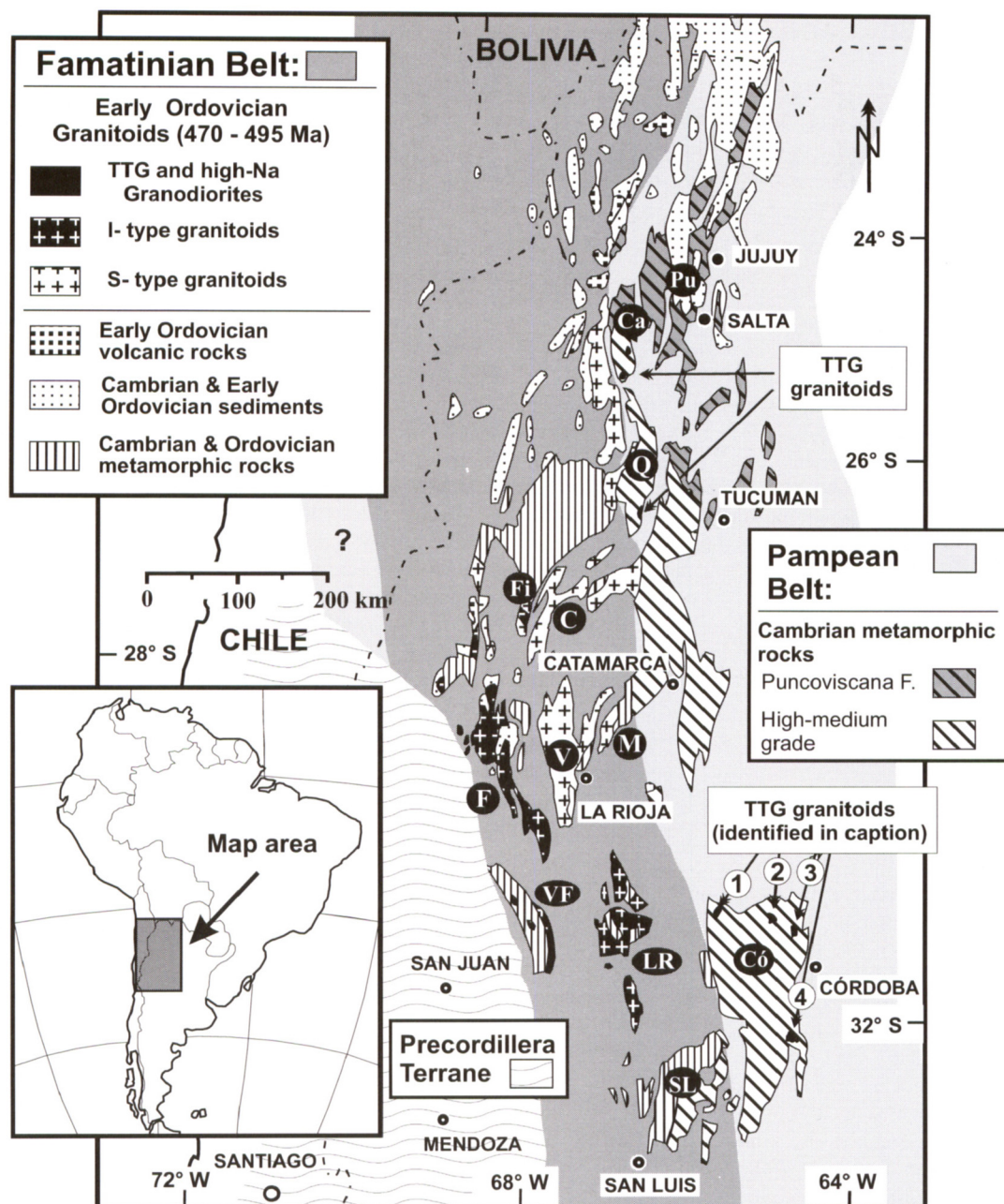


**Figure 1** Generalised sketch map of the pre-Devonian geology of the Sierras Pampeanas; the Early Palaeozoic Famatinian Belt developed on the Gondwana margin represented by the Pampean (Cambrian) basement; letters identify the main localities referred to in the text. Pu: Puna; Ca: Cachi; Q: Quilmes; Fi: Fiambalá; C: Capillitas; F: Famatina; V: Velasco; M: Mazán; VF: Valle Fértil; LR: southern La Rioja (including Los Llanos, Chepes and Ulapes); Co: Córdoba; SL: San Luis; TTG bodies in the Sierras de Córdoba are numbered: 1 = La Playa, 2 = La Fronda, 3 = Güiraldes, 4 = Calmayo and San Agustín.

## 1.2. I-type suites

Voluminous granitoids belonging to an I-type metaluminous series, ranging from gabbro to high-silica leucogranite, were emplaced in the sierras of southern La Rioja (LR in Fig. 1) and along the western side of the Famatinian belt, in the sierras of Valle Fértil and Famatina (VF and F in Fig. 1). A Middle Ordovician to Devonian age has been inferred for subvolcanic I-type plutons emplaced in a > 2000 m-thick Lower Ordovician volcano-sedimentary sequence north of 29° 20'S in the Sierra de Famatina (Cisterna 1998).

Small outcrops of low-grade metamorphic rock occur at 30–32°S, along the western margin of the Sierras de Córdoba, and in the margins and central zone of the Los Llanos–

Ulapes batholith of southern La Rioja (Pankhurst *et al.* 1998). The latter partly represent roof pendants of the country rock, and provide the only evidence for the nature of the country rocks into which these granitoids were emplaced. The sequence is predominantly metapelitic, with alternating beds of siltstone and sandstone, in which Dahlquist & Baldo (1996) demonstrated a continuous up-grade transition from phyllite in the W, through porphyroblastic schist, to gneiss, migmatite and cordierite-bearing granites in the E (in the elevated core of the sierra). They inferred thermal metamorphism at low pressures, no greater than 2.5–3 kbar (1 kbar = 100 MPa), constraining the depth of emplacement of the granitoids to a maximum of 10–12 km. Remnants of

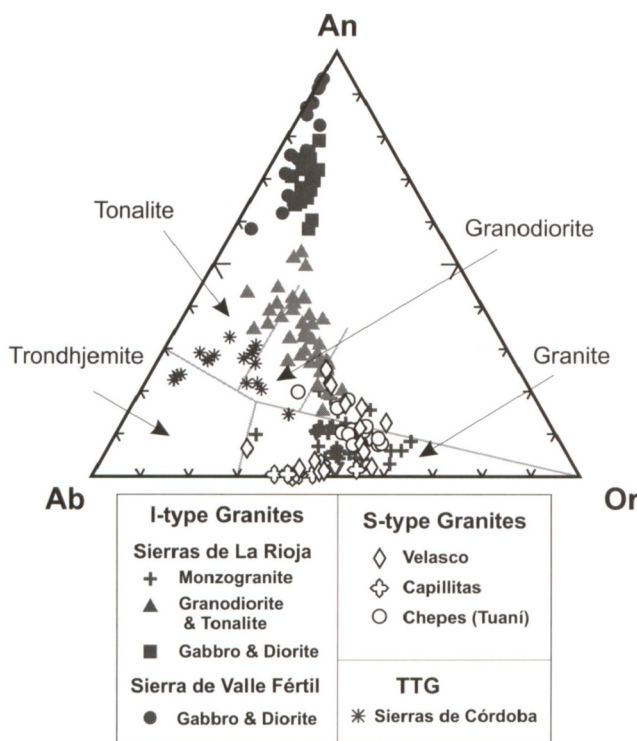


**Figure 2** Normative An–Ab–Or diagram for the granitoids rocks of the Famatinian belt.

cordierite and cordierite–garnet migmatite crop out in the Sierra de Valle Fértil, indicating similar metapelitic host rocks along the western edge of the Famatinian belt.

The I-type suites consist of three main suites: (i) gabbro, (ii) hornblende–biotite tonalite and granodiorite, and (iii) biotite monzogranite and leucogranite. The proportion and composition of gabbros changes from E to W. Whereas gabbros are scarce in the Los Llanos–Ulapes batholith, where only amphibole-bearing varieties (hornblende and cummingtonite gabbro and quartz gabbro) occur (Pascua 1998), they are ubiquitous along the western edge of the Famatinian belt. Troctolite and norite, together with hornblende gabbro, are well developed in the Sierra de Valle Fértil (Mirré 1976; Baldo *et al.* 1999), and occur discontinuously along the Sierra de Famatina (several contributions in Aceñolaza *et al.* 1996) as well as in the Sierra de Fiambalá at 27° 30' (DeBari 1994). Hornblende granodiorite, tonalite and biotite granodiorite are the dominant I-type lithologies of the Famatinian belt, and many bodies exhibit a pervasive regional cleavage. Details of their occurrence and lithology are given by Pankhurst *et al.* (1998) for the Los Llanos–Ulapes batholith and by Saavedra *et al.* (1998) for the Sierra de Famatina. Finally, small (1–5 km) bodies of true granite occur within the I-type batholiths, clearly intrusive into the main granodiorites and/or the metamorphic rocks, with sharp contacts. The common rock type is monzogranite, transitional to syenogranite, often leucocratic. Aplitic varieties occur, mostly as irregular veins. Biotite and muscovite are scarce, with apatite and zircon as the usual accessories.

### 1.3. S-type suites

S-type granites occur both as small bodies in the roof of the I-type batholiths, as in the Los Llanos–Ulapes batholith (see above), and as prominent cordierite, andalusite and two-mica bearing facies of the batholithic masses in the N of the belt, notably the Velasco, Mazán and Capillitas batholiths (V, M and C in Fig. 1). The first type appears to be associated with the high-T, low-P metamorphism affecting the metapelitic

sediments during the intrusion of I-type granodiorites (Pankhurst *et al.* 1998). It has two main facies; a fine-grained orange-brown two-mica granite with conspicuous muscovite, and a fine-grained brown cordieritic monzogranite, sometimes sillimanite or fibrolite-rich, which contains nodules of cordierite, quartz, K-feldspar and biotite, as well as numerous xenoliths of the metamorphic rocks. The accessory minerals are tourmaline (also present in the xenoliths), opaque minerals, secondary muscovite and zircon. Contacts suggest that both facies were intruded penecontemporaneously with the I-type suites (Pankhurst *et al.* 1998).

The Velasco (6000 km<sup>2</sup>) and Capillitas batholiths are among the largest of the Sierras Pampeanas (Fig. 1). Whereas these have been generally considered to be Late Ordovician to Devonian in age, based on K–Ar data (e.g. Rapela *et al.* 1992), new U–Pb SHRIMP data for the porphyritic facies (see below) indicate an Early Ordovician age, contemporaneous with the Famatinian I-type suites. Although thermobarometric studies have not been performed, a relatively shallow level of emplacement is inferred in both batholiths from contact metamorphism of low-grade shale, phyllite and schist, in which cordierite and biotite nodules are developed. Accompanying minerals are ubiquitous biotite, muscovite, cordierite, sillimanite, andalusite and tourmaline. Metasedimentary enclaves are common in most facies with aluminous minerals, including both porphyritic and two-mica granular granites. In the Sierra de Mazán, in the northeastern sector of the Velasco batholith, the local cordierite porphyritic granite is associated with a coarse pegmatoid facies with large crystals of andalusite, and quartz veins with cassiterite and wolframite. Porphyritic and granular biotite granites occur in the southwestern part of the Velasco batholith. This facies has small basic microgranular enclaves, and contains accessory allanite and sphene. Its mineralogy is transitional to the more silicic I-type varieties of the Sierras de La Rioja (Fig. 1); our data will be used to argue for a hybrid origin in both cases.

## 2. Geochemistry

The TTG, I- and S-types of Famatinian granites are easily distinguished in major and trace element plots (Figs 2, 3). The peraluminous tonalite–trondjemite–granodiorite (TTG) plutons of the Sierras de Córdoba show a restricted SiO<sub>2</sub> range of 69–75%. They are rich in Na<sub>2</sub>O and Sr, poor in FeO<sub>t</sub>, TiO<sub>2</sub>, K<sub>2</sub>O, P<sub>2</sub>O<sub>5</sub>, Cs, Rb, U, and Y, and have very low Rb/Sr ratios compared to the other granitoid groups. The bodies of Güiraldes and La Fronda (labelled as 2 and 3 respectively in Fig. 1) typically have Al<sub>2</sub>O<sub>3</sub> 14·6–16·6%, Na<sub>2</sub>O 3·3–4·3%, K<sub>2</sub>O 0·65–1·7%, FeO\*/MgO 1·5–4, Rb/Sr 0·015–0·12, [La/Yb]<sub>N</sub> 20–55, positive or absent Eu-anomalies and low contents of HREE; they plot in the adakite field of the Sr/Y vs Y diagram (Rapela *et al.* 1998).

I-types are mostly metaluminous and show a wide SiO<sub>2</sub> range of 40–79%, ASI (Alumina Saturation Index) rarely above 1·1 (Fig. 3), and a Peacock Index of 63 that corresponds to the calcic series (Pankhurst *et al.* 1998). A gap in SiO<sub>2</sub> from 54% to 57% separates the gabbroic and dioritic intrusive bodies from the dominant suites of hornblende–biotite granodiorites (Fig. 3). Given the extensive sampling, this gap is probably a real hiatus in the continuum between the more primitive compositions and the dominant metaluminous suites. However, ubiquitous mingling relationships between hornblende gabbro and tonalite–granodiorite indicate that both rock types were coeval and emplaced during the same event. The pyroxene–olivine gabbros and norites of Valle Fértil are rich in CaO and MgO and poor in incompatible elements

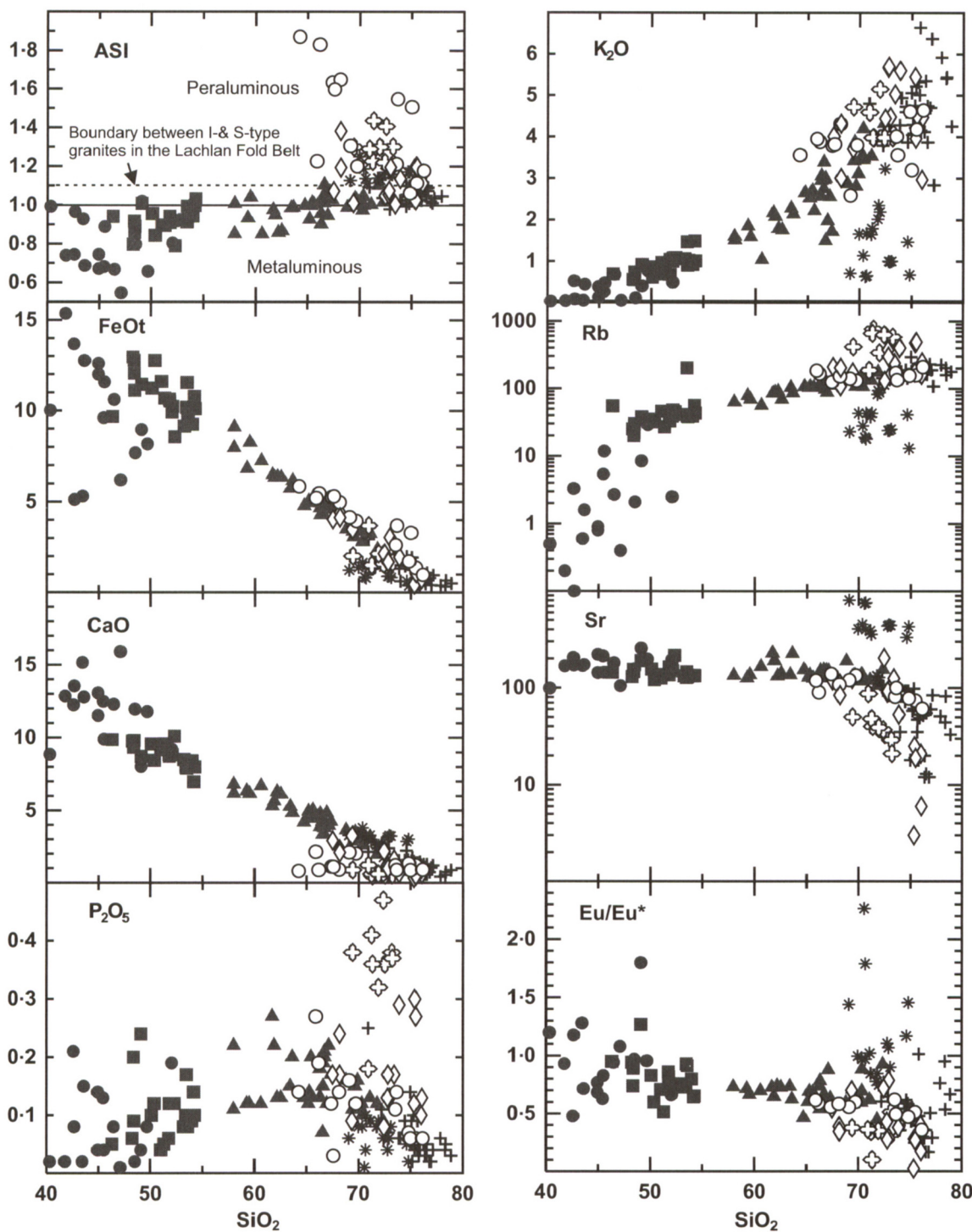


**Figure 3** Harker plots for the granitoid of the Famatinian belt; symbols as for Figure 2 (open symbols = S-type, closed symbols = I-types, asterisks = TTG).

such as K, Rb, Cs, Th, U, Zr and REE compared with the hornblende-bearing gabbros (filled circles and squares respectively in Fig. 3, Table 1). The granodiorite and tonalite units have  $K_2O$  contents of 1–5% and are generally representative of I-type batholiths formed at continental margins. Their  $SiO_2$  range is 58–72%, ASI 0.85–1.1, total alkalis 3.5–7.0%,  $[La/Yb]_N$  3–15, and they have negative Eu-anomalies (Figs 3, 10). The igneous enclaves are of tonalitic composition ( $SiO_2$  58–62%). Porphyritic biotite granodiorites (69–71%  $SiO_2$ ), which form a mappable lithological unit in the Sierras de La Rioja, are geochemically similar to the main granodiorites with respect to major elements, but are relatively rich in Ba, Rb and Sr (Pankhurst *et al.* 1998).

The most evolved members of the I-type sequences are leucocratic monzogranites with a  $SiO_2$  range of 72–79% and total alkalis 6.5–9.0%. They have slightly higher ASI (0.96–1.12) than the granodiorites, but this rarely exceeds a value of 1.1, the metaluminous-peraluminous limit for I-type granitoids of the Lachlan Fold Belt of Australia (Chappell & White 1992). Whereas some trace elements (Rb, Ga and Y) seem to lie on extensions of the granodiorite trends, others (Sr, Ba and Th) show an abrupt decrease with increasing  $SiO_2$  (Table 1). Rapid decrease of Rb and Ba in the granitic series is commonly attributed to K-feldspar and biotite fractionation (e.g. Chappell 1996; Rapela & Pankhurst 1996). The monzogranite REE patterns have  $[La/Yb]_N$  = 2.5–13 with negative Eu-

**Table 1** Selected chemical analyses of the Early Ordovician granitoids of the Famatinian Belt

Sample	I-type suites										S-type suites						TTG
	Sierra de Valle Fértil				Famatina			Sierras de La Rioja			Velasco batholith			Mazán	Capillitas batholith		La Fronda
	Troctolite	Hnb gabbro	Pyx + Hnb Ga	Hnb + Bi Gd	Hnb + Bi Gd	VCA1007	OLT-279	TUA1028	TUA1029	Crd granite	Crd granite	Bi + Mu G	LeucoG	Pegmatoid	Bi + Mu granite	LeucoT	
Sample	1 SVF602	2 SVF577	3 SVF591	4 SVF3017	5 SVF593	6 VCA1007	7 OLT-279	8 TUA1028	9 TUA1029	10 VEL3000	11 VEL1026	12 VEL3134	13 VMA1017	14 CAP1021	15 CA2485	16 LFR-82	
Major oxides (wt%)																	
SiO <sub>2</sub>	47.10	42.58	49.69	46.73	67.19	46.5	76.54	76.13	73.64	68.19	68.20	76.06	75.06	70.95	72.38	72.91	
TiO <sub>2</sub>	0.18	1.28	0.64	0.46	0.51	1.10	0.12	0.13	0.60	0.71	0.54	0.07	0.05	0.53	0.08	0.11	
Al <sub>2</sub> O <sub>3</sub>	16.19	19.05	16.75	18.65	14.64	18.07	12.79	13.18	12.71	15.36	14.66	14.00	14.30	14.22	15.02	16.21	
Fe <sub>2</sub> O <sub>3</sub>	0.95	5.19	2.30	2.07	1.85	5.70	0.27	0.66	2.40	0.52	1.78	0.39	0.45	0.80	1.76*	0.44	
FeO	5.34	9.01	6.10	6.68	2.83	7.61	0.85	0.39	1.54	3.93	2.54	0.46	0.42	2.97	n.a.	0.52	
MnO	0.13	0.23	0.16	0.17	0.11	0.23	0.06	0.07	0.10	0.10	0.07	0.04	0.07	0.07	0.04	0.02	
MgO	11.89	6.87	8.26	9.26	1.67	5.86	0.28	0.33	1.41	2.10	1.42	0.07	0.06	1.52	0.06	0.33	
CaO	15.91	12.25	11.79	12.42	4.38	10.66	1.28	0.90	0.88	2.31	2.09	0.62	0.39	1.21	0.68	3.26	
Na <sub>2</sub> O	0.44	1.69	1.97	1.02	2.75	1.82	3.17	2.76	1.68	2.23	2.32	3.70	4.95	2.35	4.12	4.25	
K <sub>2</sub> O	0.05	0.52	0.76	0.32	2.63	0.89	3.87	4.64	3.56	3.01	4.32	4.47	2.02	4.59	3.98	0.99	
P <sub>2</sub> O <sub>5</sub>	0.01	0.21	0.08	0.07	0.13	0.19	0.05	0.06	0.14	0.17	0.24	0.13	0.36	0.18	0.47	0.06	
H <sub>2</sub> O+	0.87	0.98	1.48	0.95	0.50	0.94	0.58	0.49	1.02	0.40	1.16	0.34	0.69	0.87	0.08	0.68	
H <sub>2</sub> O-	0.18	0.05	0.13	0.15	0.20	0.08	0.15	0.15	0.20	0.30	0.40	0.08	0.15	0.14	0.80	0.12	
Total	99.11	99.91	100.11	98.85	99.39	99.65	100.01	99.89	99.88	99.37	99.74	100.43	98.97	100.4	99.47	99.90	
Trace elements (ppm)																	
Cs	0.4	0.2	1	<0.1	2.6	1.5	3.9	11	6.1	2.4	3.5	2.2	187	8.6	61.1	0.4	
Rb	0.4	3.3	29	3	111	30	162	209	134	108	203	246	495	186	629	24	
Sr	105	205	198	231	123	235	55	61	100	110	84	6	11	87	37	447	
Ba	20	70	114	48	344	135	236	284	499	420	308	4	9	379	55	240	
La	1.2	15.6	7.7	4.36	27.2	15.8	18.2	22.9	41.1	55.2	39.4	3.12	2.82	47.5	4.9	21.3	
Ce	3	54	18	11	56	44.6	42	49.8	84.5	117	85.8	7	7.3	104	11	42	
Pr	n.a.	n.a.	n.a.	1.59	n.a.	5.97	n.a.	5.29	9.04	13.7	9.28	0.83	0.91	11.44	n.a.	n.a.	
Nd	2	38	9	7.41	24	26.9	20	19.1	34.1	51.5	34.6	2.96	3.21	43.1	5	16	
Sm	0.48	9.38	1.96	1.88	4.68	6.19	4.41	4.49	6.87	10.8	7.78	1.05	1.26	9.05	1.21	2.1	
Eu	0.19	1.58	0.63	0.60	0.96	1.42	0.57	0.57	1.14	1.47	0.95	0.08	0.01	1.08	0.16	0.8	
Gd	n.a.	n.a.	n.a.	1.86	n.a.	5.35	n.a.	3.90	5.34	10.7	7.06	1.22	0.96	7.03	n.a.	n.a.	
Tb	0.1	1.7	0.3	0.33	0.9	0.96	0.9	0.84	1.03	1.94	1.46	0.36	0.25	1.28	0.3	0.2	
Dy	n.a.	n.a.	n.a.	1.88	n.a.	5.47	n.a.	5.08	5.82	10.7	8.36	2.22	1.34	6.86	n.a.	n.a.	
Ho	n.a.	n.a.	n.a.	0.41	n.a.	1.09	n.a.	1.07	1.20	2.08	1.46	0.44	0.20	1.35	n.a.	n.a.	
Er	n.a.	n.a.	n.a.	1.19	n.a.	3.17	n.a.	3.33	3.59	5.01	3.68	1.34	0.57	3.94	n.a.	n.a.	
Tm	n.a.	n.a.	n.a.	0.17	n.a.	0.47	n.a.	0.56	0.55	0.58	0.47	0.27	0.13	0.57	n.a.	n.a.	
Yb	0.44	5.54	1.27	1.01	3.14	2.96	4.75	3.80	3.65	2.84	2.54	2.10	1.09	3.23	0.51	0.6	
Lu	0.06	0.79	0.17	0.15	0.42	0.44	0.65	0.58	0.55	0.36	0.32	0.28	0.15	0.44	0.06	0.1	
U	—	0.1	0.1	0.09	0.9	0.17	2.1	4.09	3.03	1.48	1.26	4.63	3.10	2.48	5.2	0.5	
Th	—	0.4	2.3	0.5	7.7	0.45	9.5	18.6	13.9	21.1	16.2	1.62	1.63	22.2	2.7	4.5	
Y	6	58	17	10.3	35	27	47	33	34	55.3	43	12.7	7	36	30	5	
Nb	1	5	2	1.4	12	8	13	17	15	13.3	17	11.7	30	14	34	3	
Zr	18	120	17	17	142	101	73	84	233	276	182	21	29	188	40	93	
Hf	0.2	3.6	1	0.6	4	2.9	2.4	2.7	7.3	7.5	4.9	1.3	1.8	5.6	1.3	2	
Ta	—	0.2	0.1	<0.1	1.9	1.15	4.48	4.26	0.5	3.55	1.53	9.31	3.3	4.7	1		
Sc	53.5	60	33	44	19	43	6.5	6	12	10	15	3	9	11	4.8	1.2	
Ga	5	21	11	15	15	21	12	13	16	20	18	16	25	18	26	16	
Co	43.2	47.5	29.9	46	33	53	1.8	28	51	13	32	5	40	33	1.5	2	
Cr	1010	76.6	190	88	24	59	22.3	105	43	86	50	316	55	44	16.3	8	

Notes: \*Fe<sub>2</sub>O<sub>3</sub> total; n.a. = not analysed; Pyx = pyroxene; Hnb = hornblende; Bi = biotite; Mu = muscovite; Crd = cordierite; Ga = gabbro; G = granite; T = tonalite. Fe<sup>++</sup> determined volumetrically at Centro de Investigaciones Geológicas, La Plata. Samples 3,6,8,9,10,11,12,13,14 analysed by ICP and ICP-MS and samples 1,2,4,5,7,15 by XRF on fusion pellets (major elements) and INAA (trace elements), at ACTLABS (Canada).

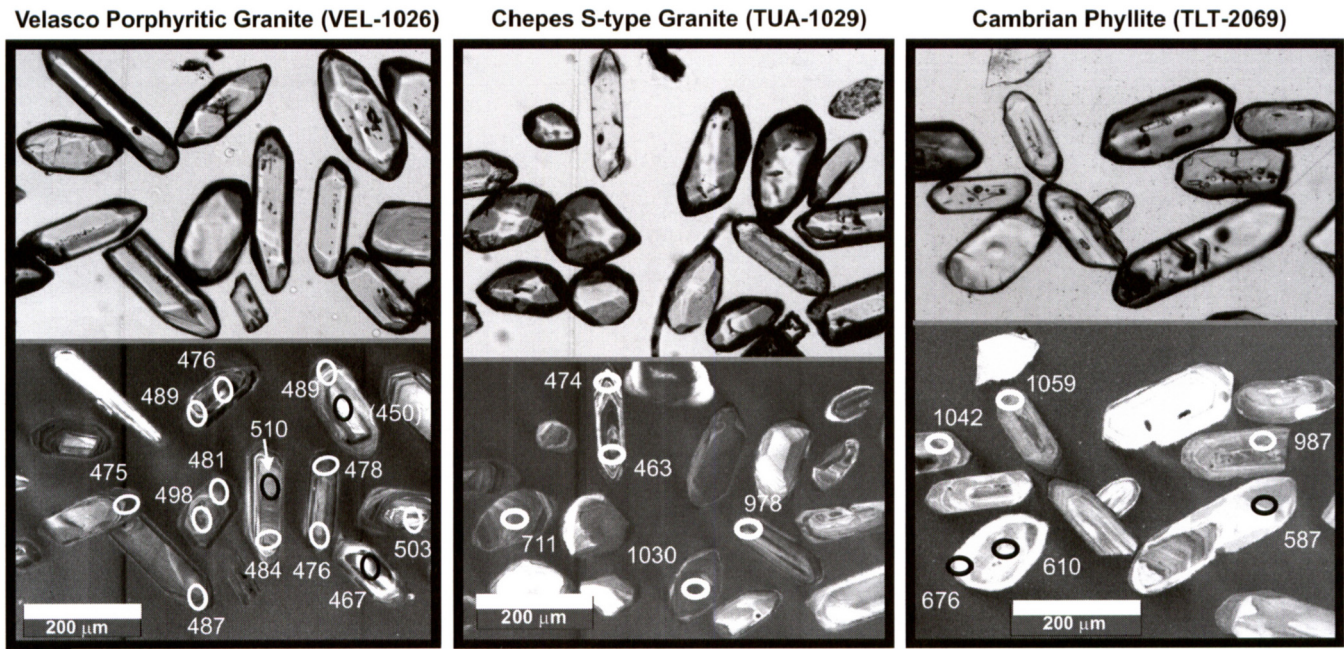


**Figure 4** Illustrative optical and cathodo-luminescence images of parts of the zircon mounts used in this study, with the ages of spot analyses indicated in Ma.

anomalies. The aplites on the other hand have relatively flat REE patterns ( $[La/Yb]_N = 0.5\text{--}1.5$ ) and are depleted in total REE compared to the granodiorites, probably due to fractionation of a REE-rich accessory phase such as allanite, which is conspicuous in the dominant hornblende–biotite granodiorite facies.

The S-type granites show a restricted silica range of 64–76%  $SiO_2$  and most samples have ASI values higher than 1.1 (Fig. 3). Compared to I-types and TTG in the same silica interval, all S-types are poor in CaO and Sr, and rich in  $P_2O_5$ , Rb and  $K_2O$ . Rb correlates positively with Cs, and the Capillitas granites with 800–1000 ppm of Rb have 70–100 ppm of Cs. The largest negative Eu-anomalies occur in the S-type granites (Fig. 3).

The highest ASI values (1.5–1.8) and least silicic varieties are found in the cordierite granites of the sierras of southern La Rioja (Tuaní Granite, Pankhurst *et al.* 1998). These restricted bodies were probably formed by melting of adjacent high-grade metapelites (see section 4), and their high ASI index reflects their restite-rich *in situ* origin.  $[La/Yb]_N$  values of 6.0–7.8, accompanied by negative Eu-anomalies, are indistinguishable from those of the locally associated metamorphic rocks (see fig. 9 of Pankhurst *et al.* 1998). On the other hand, the dominant porphyritic facies of Velasco and Capillitas batholiths has  $SiO_2$  67–73%, REEt 130–330 ppm,  $[La/Yb]_N$  3–14, and Eu/Eu\* 0.35–0.8. Associated leucogranites have the most extreme compositions among the S-types, with 75–76%  $SiO_2$ , low REEt content (20–60 ppm),  $[La/Yb]_N$  1–3 and Eu/Eu\* 0.02–0.4. Cordierite, andalusite, sillimanite and two-mica facies of Capillitas and Velasco have ASI values in the interval 1.2–1.4, whereas the biotite facies of the southwestern part of Velasco has ASI values between 1.0 and 1.1, consistent with its weakly peraluminous mineralogy and mafic microgranular enclaves.

### 3. U–Pb SHRIMP geochronology

U–Pb ages were determined on zircon mounts using the SHRIMP microprobe at ANU (see Compston *et al.* 1992). In

order to define magmatic crystallisation ages, analysis spots were targeted in zoned rims and overgrowths, whereas for the determination of inheritance patterns, pre-magmatic zircon cores were analysed. Illustrative images for three samples are shown in Figure 4. The new results are summarised in Table 2 and representative U–Pb Concordia plots are shown in Figures 5–7. Once consistent data sets were identified from this diagram, the measured  $^{207}Pb$  was used to correct for common Pb, and a final result was obtained by calculating the weighted mean  $^{238}U$ – $^{206}Pb$  age. Errors are quoted at the 95% confidence level.

#### 3.1. Tonalite–trondhjemite–granodiorite suite

Lork *et al.* (1991) reported U–Pb monazite ages of  $466 \pm 1$  to  $481 \pm 1$  Ma for trondhjemites in the Sierra de Cachi. Geochronological evidence for the age of the TTG suite in the Sierras Pampeanas was presented by Rapela *et al.* (1998). Trondhjemite from the Güiraldes body in the Sierras de

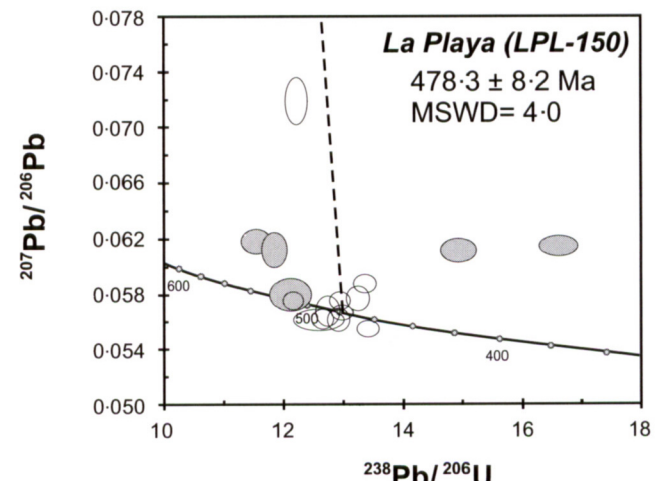


**Figure 5** Tera-Wasserburg U–Pb diagram for the La Playa granodiorite, considered to belong to the TTG group; error ellipses are  $1\sigma$ ; shaded points are excluded from the age calculation; the dotted line shows the projected composition of common Pb at the time of crystallisation.

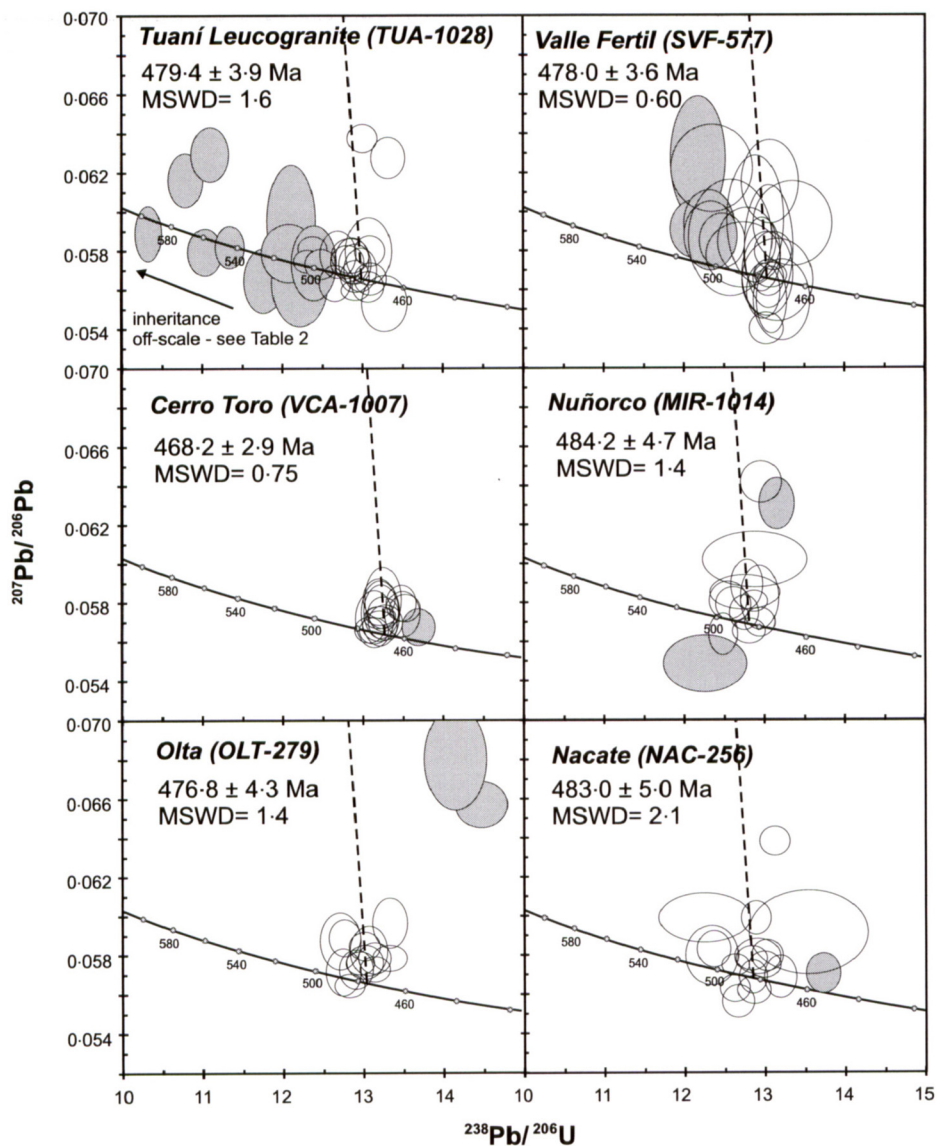


Figure 6 Tera-Wasserburg diagrams for I-type Famatinian granitoids; comments as for Figure 5.

Córdoba gave a conventional U-Pb zircon age of  $496 \pm 2$  Ma, and U-Pb SHRIMP zircon data gave a concordant result of  $499 \pm 5$  Ma (both also exhibited evidence of Precambrian inheritance in the magma). Rb-Sr whole-rock data listed by the same authors for four trondhjemite samples (all with very low Rb/Sr ratios) and one aplite from the La Fronda body give an isochron age of  $483 \pm 5$  Ma (initial  $^{87}\text{Sr}/^{86}\text{Sr}$  ratio  $0.7063$ , MSWD 0.3). The granodiorite of La Playa, which also fell on this isochron, has now yielded a U-Pb zircon age of  $478 \pm 8$  Ma (Fig. 5). The data are rather scattered, as indicated by the MSWD of 4.0; this appears to be due in part to a number of results close to 500 Ma, which were ignored in the age calculation.

These ages are significantly younger than that of magmatism associated with the Pampean event (520–530 Ma); they indicate that the TTG magmatism in this area was of Ordovician age, probably one of the earliest plutonic events in the Famatinian arc.

### 3.2. I-type granitoids

Two of the results shown in Figure 6 are for I-type granitoids from the collection of Pankhurst *et al.* (1998) from the Sierra de Chepes (Fig. 1). NAC-256 is a hornblende-biotite grano-

diorite representative of the Chepes Granodiorite unit, which yielded scattered Rb-Sr data but consistent U-Pb zircon ages of  $486 \pm 4$  Ma (conventional) and  $497 \pm 7$  Ma (SHRIMP). The new result of  $483 \pm 5$  Ma is indistinguishable from the previous conventional age. This suggests that either the emplacement of this voluminous unit took place over a significant period of time, or that the older SHRIMP age ( $497 \pm 5$  Ma) was biased by unresolved inheritance. OLT-279 is a sample of the later monzogranitic phase in the Sierra de Chepes (Asperezas Granite unit) that fell on the youngest Rb-Sr errorchron obtained in the previous study ( $452 \pm 11$  Ma, Pankhurst *et al.* 1998). The Rb-Sr result is superseded by the U-Pb SHRIMP age of  $477 \pm 4$  Ma, which confirms that these granites are only marginally younger than the far more voluminous granodiorites into which they were emplaced. A third sample from this area is TUA-1028, a leucogranite associated with an S-type cordierite granite; it has a significant proportion of inherited zircon (Table 2) with provenance ages of 500, 560, 600, 650, 850, 1050, 1120 and 1610 Ma (Table 2). The intrusive age determined from the remaining data (Fig. 6) is  $479 \pm 4$  Ma.

Two samples were dated from the Sierra de Valle Fértil in the western Sierras Pampeanas (Fig. 1). SVF-577, a slightly altered hornblende gabbro, also shows signs of inherited zircon,

Table 2 SHRIMP U-Pb zircon data

Grain spot	U ppm	Th ppm	Th/U	Pb* ppm	$^{204}\text{Pb}/^{206}\text{Pb}$	$f_{206}$ %	Measured ratios			Radiogenic		Age (Ma)		
							$^{238}\text{U}/^{206}\text{Pb}$	s.d.	$^{207}\text{Pb}/^{206}\text{Pb}$	s.d.	$^{206}\text{Pb}/^{238}\text{U}$	s.d.	$^{206}\text{Pb}/^{238}\text{U}$	s.d.
<b>1. Trondjemite-tonalite-granodiorite Group</b>														
Sample LPL-150, Two-mica granodiorite, La Playa, Sierra Grande de Córdoba ( $30^{\circ} 59' 01''\text{S}$ ; $65^{\circ} 23' 26''\text{W}$ )														
1-1	538	375	0.70	55	0.000010	<0.01	13.414	0.15510	0.05551	0.00049	0.0747	0.0009	464.2	5.2
2-1	672	97	0.14	63	0.000061	<0.01	12.588	0.34732	0.05616	0.00064	0.0795	0.0022	493.1	13.1
3-1	435	317	0.73	45	0.000078	0.12	13.243	0.15472	0.05771	0.00072	0.0754	0.0009	468.7	5.3
4-1	620	507	0.82	66	—	0.00	12.977	0.14540	0.05668	0.00044	0.0771	0.0009	478.6	5.2
5-1	535	455	0.85	56	0.000181	0.26	13.358	0.16032	0.05879	0.00054	0.0747	0.0009	464.2	5.4
6-1	494	283	0.57	54	0.000049	<0.01	12.161	0.14171	0.05754	0.00051	0.0823	0.0010	509.5	5.7*
7-1	541	464	0.86	64	0.000051	0.03	12.123	0.28788	0.05802	0.00097	0.0825	0.0020	510.8	11.7*
8-1	710	623	0.88	77	0.000031	0.10	12.947	0.14303	0.05753	0.00055	0.0772	0.0009	479.2	5.1
9-1	202	104	0.52	22	0.000199	0.43	11.857	0.17820	0.06122	0.00102	0.0840	0.0013	519.8	7.5*
10-1	333	252	0.76	40	0.000386	0.50	11.546	0.20225	0.06181	0.00074	0.0862	0.0015	532.9	9.0*
11-1	764	301	0.39	65	0.000334	0.55	14.934	0.24061	0.06117	0.00070	0.0666	0.0011	415.6	6.5*
12-1	239	209	0.88	26	—	<0.01	12.918	0.15320	0.05616	0.00069	0.0775	0.0009	481.0	5.5
13-1	461	320	0.69	36	0.000297	0.59	16.610	0.27391	0.06149	0.00061	0.0599	0.0010	374.7	6.0*
14-1	624	432	0.69	68	0.000096	<0.01	12.655	0.14768	0.05621	0.00060	0.0791	0.0009	490.6	5.5
15-1	412	181	0.44	42	0.000791	1.87	12.219	0.15625	0.07186	0.00136	0.0803	0.0010	498.0	6.2
16-1	183	154	0.84	20	0.000230	0.01	12.738	0.16742	0.05679	0.00091	0.0785	0.0010	487.2	6.2
MSWD = 4.0										Weighted mean		478.0	1.8	
<b>2. I-type granite Group</b>														
Sample NAC-256 Hornblende-biotite granodiorite, Nacate, Sierra de Chepes, ( $30^{\circ} 54' 28''\text{S}$ ; $66^{\circ} 23' 55''\text{W}$ )														
1-1	611	223	0.37	60	—	<0.01	12.623	0.15038	0.05629	0.00057	0.0793	0.0010	491.7	5.7
2-1	253	135	0.53	24	0.000010	0.05	13.729	0.17650	0.05706	0.00081	0.0728	0.0009	453.0	5.6*
3-1	468	302	0.65	47	0.000567	0.88	13.125	0.15528	0.06382	0.00059	0.0755	0.0009	469.3	5.4
4-1	263	337	1.28	32	—	<0.01	12.664	0.16134	0.05562	0.00068	0.0791	0.0010	490.6	6.0
5-1	254	256	1.01	29	0.000057	0.15	12.904	0.23163	0.05791	0.00074	0.0774	0.0014	480.5	8.3
6-1	417	324	0.78	46	0.000096	0.20	12.362	0.17331	0.05828	0.00076	0.0807	0.0011	500.5	6.8
7-1	444	180	0.40	43	0.000016	0.10	12.988	0.16212	0.05749	0.00055	0.0769	0.0010	477.7	5.8
8-1	296	286	0.97	33	0.000243	0.15	13.015	0.16602	0.05795	0.00064	0.0767	0.0010	476.5	5.9
9-1	200	140	0.70	22	0.000217	0.16	12.339	0.26910	0.05796	0.00124	0.0809	0.0018	501.6	10.6
10-1	405	225	0.56	41	0.000090	<0.01	12.863	0.16617	0.05620	0.00060	0.0778	0.0010	482.9	6.0
11-1	172	202	1.17	19	0.000010	0.30	13.537	0.60915	0.05912	0.00174	0.0737	0.0033	458.1	20.0
12-1	600	334	0.56	61	0.000066	0.14	12.834	0.15704	0.05780	0.00050	0.0778	0.0010	483.1	5.7
13-1	696	451	0.65	74	0.000061	0.10	12.632	0.14192	0.05747	0.00044	0.0791	0.0009	490.7	5.3
14-1	890	652	0.73	98	0.000223	0.39	12.247	0.46575	0.05988	0.00103	0.0813	0.0031	504.1	18.5
15-1	477	293	0.62	48	0.000040	0.02	13.189	0.16274	0.05686	0.00088	0.0758	0.0009	471.0	5.6
16-1	787	269	0.34	75	0.000024	0.02	12.849	0.14571	0.05688	0.00069	0.0778	0.0009	483.1	5.3
17-1	349	419	1.20	41	0.000237	0.39	12.889	0.15319	0.05989	0.00071	0.0773	0.0009	479.9	5.5
MSWD = 2.1										Weighted mean		483.0	2.5	
Sample OLT-279 Biotite monzogranite, Olta, Sierra de Los Llanos ( $30^{\circ} 37' 57''\text{S}$ ; $66^{\circ} 19' 37''\text{W}$ )														
1-1	281	185	0.66	22	0.000222	0.20	13.013	0.15660	0.05848	0.00060	0.0767	0.0009	476.3	5.5
2-1	392	449	1.15	35	0.000177	0.06	13.143	0.15805	0.05733	0.00052	0.0760	0.0009	472.5	5.5
3-1	284	327	1.15	25	0.000309	0.18	13.070	0.19463	0.05826	0.00104	0.0764	0.0011	474.5	6.8
4-1	229	316	1.38	22	0.000214	0.10	13.023	0.18833	0.05767	0.00071	0.0767	0.0011	476.4	6.7
5-1	489	176	0.36	36	0.000010	0.10	12.959	0.14698	0.05761	0.00047	0.0771	0.0009	478.7	5.2
6-1	747	334	0.45	58	—	<0.01	12.826	0.15397	0.05647	0.00048	0.0780	0.0009	484.2	5.6
7-1	192	135	0.70	15	0.000794	0.35	13.335	0.17887	0.05967	0.00106	0.0747	0.0010	464.6	6.0
8-1	131	95	0.72	11	0.000082	0.24	12.706	0.20800	0.05876	0.00120	0.0785	0.0013	487.3	7.7
9-1	91	104	1.14	7	0.000043	1.39	14.159	0.31830	0.06810	0.00213	0.0696	0.0016	434.0	9.5*
10-1	212	165	0.78	18	0.000137	0.26	12.766	0.16701	0.05893	0.00078	0.0781	0.0010	485.0	6.1
11-1	296	247	0.83	25	0.000279	0.06	12.907	0.17200	0.05731	0.00082	0.0774	0.0010	480.8	6.2
12-1	187	134	0.72	16	0.000311	0.04	12.745	0.18529	0.05717	0.00097	0.0784	0.0011	486.8	6.8
13-1	446	325	0.73	36	0.000109	0.13	13.328	0.17523	0.05788	0.00055	0.0749	0.0010	465.8	5.9
14-1	218	270	1.24	20	0.000223	0.13	13.140	0.16913	0.05788	0.00065	0.0760	0.0010	472.2	5.9
15-1	183	119	0.65	12	0.001146	1.10	14.423	0.21617	0.06577	0.00093	0.0686	0.0010	427.5	6.2*
MSWD = 1.4										Weighted mean		476.8	1.7	
Sample TUA-1028 Tuaní leucogranite, Sierra de Chepes ( $31^{\circ} 08' 00''\text{S}$ ; $66^{\circ} 32' 50''\text{W}$ )														
<b>SHRIMP II</b>														
1-1	164	132	0.81	20	0.000010	0.54	11.103	0.19340	0.06292	0.00115	0.0896	0.0016	553.1	9.3*
2-1	281	230	0.82	35	0.000033	<0.01	11.349	0.15146	0.05818	0.00088	0.0882	0.0012	544.6	7.0*
3-1	538	48	0.09	50	0.000133	0.17	12.378	0.14450	0.05812	0.00051	0.0807	0.0009	500.0	5.6*
4-1	146	147	1.01	16	0.000289	0.10	12.872	0.17406	0.05748	0.00095	0.0776	0.0011	481.9	6.3
5-1	85	80	0.94	10	0.000010	0.08	12.400	0.23293	0.05737	0.00157	0.0806	0.0015	499.6	9.1*
5-2	732	305	0.42	71	—	<0.01	12.909	0.14312	0.05595	0.00042	0.0775	0.0009	481.4	5.2
6-1	293	244	0.83	32	—	0.09	12.812	0.17255	0.05741	0.00069	0.0780	0.0011	484.1	6.3
7-1	272	100	0.37	25	0.000257	0.75	13.321	0.17603	0.06276	0.00087	0.0745	0.0010	463.3	5.9
8-1	406	266	0.65	42	0.000010	<0.01	13.073	0.16211	0.05616	0.00063	0.0766	0.0010	475.5	5.7
9-1	160	185	1.16	19	0.000195	0.04	12.979	0.16635	0.05701	0.00091	0.0770	0.0010	478.3	5.9
10-1	327	44	0.14</											

Table 2 (continued)

Grain spot	U ppm	Th ppm	Th/U	Pb* ppm	$^{204}\text{Pb}/$ $^{206}\text{Pb}$	$f_{206}$ %	Measured ratios				Radiogenic		Age (Ma)						
							$^{238}\text{U}/$ $^{206}\text{Pb}$	s.d.	$^{207}\text{Pb}/$ $^{206}\text{Pb}$	s.d.	$^{206}\text{Pb}/$ $^{238}\text{U}$	s.d.	$^{206}\text{Pb}/$ $^{238}\text{U}$	s.d.					
<b>2. I-type granite Group (continued)</b>																			
Sample TUA-1028 (continued)																			
<i>SHRIMP I</i>																			
6·2	241	247	1·02	16	0·000168	<0·01	13·273	0·23437	0·05528	0·00120	0·0755	0·0013	469·0	8·0					
7·2	173	115	0·66	12	0·000010	<0·01	12·234	0·28988	0·05631	0·00187	0·0819	0·0020	507·2	11·6*					
17·2	361	296	0·82	32	0·000256	<0·01	9·473	0·18875	0·06036	0·00106	0·1057	0·0021	647·6	12·3*					
18·2	521	270	0·52	37	0·000010	<0·01	11·043	0·17216	0·05790	0·00099	0·0907	0·0014	559·4	8·4*					
19·2	537	134	0·25	55	0·000062	0·10	7·129	0·11439	0·06787	0·00060	0·1402	0·0023	845·5	12·7*					
21·2	147	134	0·91	10	0·000036	0·25	12·116	0·24467	0·05948	0·00235	0·0823	0·0017	510·0	10·0*					
22·1	200	52	0·26	12	0·000317	<0·01	13·416	0·28634	0·01624	0·00142	0·0783	0·0017	485·7	10·0					
22·2	165	47	0·28	10	0·000010	<0·01	12·595	0·30683	0·02815	0·00162	0·0823	0·0020	509·6	12·0*					
23·1	168	77	0·46	39	0·000120	0·18	3·524	0·08202	0·10081	0·00385	0·2833	0·0067	1607·7	33·8*					
24·1	194	253	1·31	15	—	0·05	12·092	0·28042	0·05786	0·00123	0·0827	0·0019	512·0	11·5*					
25·1	382	69	0·18	23	0·000100	<0·01	11·778	0·20635	0·05639	0·00136	0·0851	0·0015	526·5	8·9*					
26·1	125	87	0·69	19	0·000248	0·43	5·246	0·13803	0·07908	0·00147	0·1898	0·0050	1120·3	27·2*					
27·1	72	82	1·13	12	0·000382	0·20	5·656	0·17452	0·07598	0·00244	0·1765	0·0055	1047·6	30·0*					
27·2	484	124	0·26	32	0·000026	0·34	10·799	0·17513	0·06159	0·00114	0·0923	0·0015	569·0	8·9*					
										MSWD = 1·6	Weighted mean		479·4	1·5					
Sample SVF-577 Hornblende gabbro, Sierra de Valle Fertil ( $30^{\circ} 39' 28''\text{S}$ ; $67^{\circ} 36' 17''\text{W}$ )																			
<i>SHRIMP I</i>																			
1·1	86	31	0·37	7	—	<0·01	13·203	0·28934	0·05553	0·00169	0·0759	0·0017	471·4	10·0					
2·1	154	61	0·40	13	—	<0·01	13·080	0·15603	0·05553	0·00139	0·0766	0·0009	475·7	5·5					
3·1	135	80	0·59	13	0·000536	0·20	12·462	0·23229	0·05855	0·00115	0·0801	0·0015	496·6	8·9*					
4·1	133	63	0·47	12	—	0·11	12·722	0·37818	0·05783	0·00136	0·0785	0·0023	487·3	14·0					
5·1	48	27	0·56	4	0·001276	0·33	12·885	0·28591	0·05967	0·00264	0·0774	0·0017	480·3	10·4					
6·1	74	41	0·55	7	—	<0·01	13·150	0·36263	0·05654	0·00172	0·0761	0·0021	472·7	12·6					
7·1	38	22	0·59	4	0·000010	0·21	12·563	0·42329	0·05868	0·00244	0·0794	0·0027	492·7	16·1*					
8·1	75	32	0·42	7	0·000668	0·72	12·167	0·28054	0·06279	0·00260	0·0816	0·0019	505·7	11·3*					
9·1	79	44	0·55	7	0·001232	0·31	13·345	0·40332	0·05944	0·00176	0·0747	0·0023	464·4	13·6					
10·1	98	62	0·63	10	0·000600	0·31	12·300	0·25726	0·05945	0·00138	0·0811	0·0017	502·4	10·2*					
11·1	67	31	0·47	6	0·001100	0·65	12·331	0·41382	0·06224	0·00181	0·0806	0·0027	499·5	16·2					
12·1	107	62	0·58	10	0·000583	<0·01	13·028	0·25785	0·05686	0·00175	0·0768	0·0015	476·8	9·2					
13·1	117	59	0·50	11	—	0·23	12·320	0·26888	0·05881	0·00145	0·0810	0·0018	502·0	10·6*					
14·1	112	69	0·62	10	0·000627	0·19	12·774	0·29773	0·05850	0·00142	0·0781	0·0018	485·0	10·9					
15·1	142	97	0·68	14	0·000213	0·27	12·121	0·25262	0·05916	0·00120	0·0823	0·0017	509·7	10·3*					
<i>SHRIMP II</i>										MSWD = 0·33	Weighted mean		476·9	1·9					
Sample SVF-593 Hornblende-biotite granodiorite, La Majadita, Sierra de Valle Fertil ( $30^{\circ} 40' 21''\text{S}$ ; $67^{\circ} 30' 30''\text{W}$ )																			
1·1	415	272	0·66	33	0·000275	0·22	13·944	0·18496	0·05845	0·00076	0·0737	0·0010	458·2	5·9					
2·1	529	498	0·94	47	0·000034	<0·01	13·434	0·15689	0·05644	0·00062	0·0767	0·0009	476·1	5·4					
3·1	268	129	0·48	21	—	0·05	13·539	0·16466	0·05711	0·00079	0·0760	0·0009	472·2	5·6					
4·1	394	210	0·53	31	0·000305	0·21	13·904	0·18664	0·05837	0·00075	0·0739	0·0010	459·5	6·0					
5·1	345	185	0·54	28	0·000011	0·24	13·576	0·16684	0·05866	0·00080	0·0756	0·0009	470·1	5·6					
6·1	457	226	0·49	37	0·000160	<0·01	13·193	0·22770	0·05600	0·00062	0·0781	0·0014	484·8	8·1					
7·1	624	641	1·03	54	0·000157	0·17	14·125	0·16985	0·05809	0·00046	0·0728	0·0009	452·7	5·3*					
8·1	527	292	0·55	35	0·000614	0·73	16·473	0·29596	0·06258	0·00095	0·0620	0·0011	388·0	6·8*					
9·1	325	426	1·31	31	0·000087	0·27	13·752	0·16816	0·05886	0·00068	0·0747	0·0009	464·2	5·5					
10·1	313	350	1·12	29	—	0·20	13·595	0·17610	0·05829	0·00108	0·0756	0·0010	469·6	5·9					
11·1	510	504	0·99	47	0·000257	0·04	13·400	0·16567	0·05704	0·00047	0·0768	0·0010	476·9	5·7					
12·1	217	138	0·63	18	0·000101	0·20	13·705	0·21552	0·05830	0·00103	0·0750	0·0012	466·0	7·1					
13·1	414	478	1·15	40	0·000043	<0·01	13·118	0·25295	0·05646	0·00072	0·0785	0·0015	487·1	9·1					
14·1	396	354	0·89	34	0·000044	0·17	13·842	0·22965	0·05804	0·00077	0·0742	0·0012	461·7	7·4					
15·1	352	200	0·57	27	0·000247	0·28	14·322	0·19757	0·05897	0·00095	0·0717	0·0010	446·2	6·0*					
16·1	363	321	0·88	31	0·000102	0·31	13·679	0·42760	0·05923	0·00080	0·0750	0·0024	466·3	14·1					
								MSWD = 1·6	Weighted mean				469·5	1·8					
Sample VCA-1007 Gabbro-diorite, Villa Castelli ( $28^{\circ} 58' 49''\text{S}$ ; $68^{\circ} 13' 07''\text{W}$ )																			
1·1	173	75	0·43	15	0·000836	0·21	13·245	0·18595	0·05814	0·00134	0·0753	0·0011	468·3	6·4					
2·1	200	62	0·31	17	0·00171	0·03	13·687	0·16788	0·05672	0·00077	0·0730	0·0009	454·4	5·4*					
3·1	452	357	0·79	43	0·000074	0·18	13·474	0·15255	0·05794	0·00076	0·0741	0·0008	460·7	5·1					
4·1	364	236	0·65	33	0·000115	0·16	13·521	0·15844	0·05770	0·00057	0·0739	0·0009	459·3	5·2					
5·1	434	310	0·71	41	0·000026	0·13	13·247	0·15536	0·05746	0·00066	0·0754	0·0009	468·6	5·3					
6·1	293	218	0·74	28	—	0·04	13·207	0·17801	0·05678	0·00064	0·0757	0·0010	470·3	6·1					
7·1	216	122	0·56	20	0·000146	0·06	13·275	0·17475	0·05696	0·00074	0·0753	0·0010	467·9	6·0					
8·1	402	306	0·76	39	0·000010	0·02	13·071	0·14970	0·05658	0·00053	0·0765	0·0009	475·2	5·3					
9·1	496	366	0·74	47	0·000068	0·09	13·193	0·15367	0·05721	0·00047	0·0757	0·0009	470·6	5·3					
10·1	180	105	0·58	17	—	0·13	13·220	0·17554	0·05753	0·00112	0·0755	0·0010	469·4	6·1					
11·1	807	862	1·07	83	0·000034	0·11	13·213	0·15198	0·05730	0·00040	0·0756	0·0009	469·8	5·2					
12·1	347	251	0·72	33	0·000049	0·01	13·131	0·15039	0·05654	0·00055	0·0762	0·0009	473·1	5·2					
13·1	155	95	0·61	14	0·000010	0·12	13·209	0·19667	0·05743	0·00136	0·0756	0·0011	469·9	6·8					
14·1	198	132	0·67	19	0·000149	0·08	13·137	0·19559	0·05713										

Table 2 (continued)

Grain spot	U ppm	Th ppm	Th/U	Pb* ppm	$^{204}\text{Pb}/^{206}\text{Pb}$	$f_{206}$ %	Measured ratios				Radiogenic		Age (Ma)							
							$^{238}\text{U}/^{206}\text{Pb}$	s.d.	$^{207}\text{Pb}/^{206}\text{Pb}$	s.d.	$^{206}\text{Pb}/^{238}\text{U}$	s.d.	$^{206}\text{Pb}/^{238}\text{U}$	s.d.						
<b>2. I-type granite Group (continued)</b>																				
Sample MIR-1014 Biotite granodiorite, Nuñorco Granite, Cuesta de Miranda, Famatina (29° 20' 30"S; 67° 46' 22"W)																				
1·1	515	294	0·57	52	0·000087	0·03	12·934	0·15624	0·05698	0·00061	0·0773	0·0009	479·9	5·6						
2·1	372	256	0·69	40	0·000087	0·17	12·537	0·19209	0·05807	0·00081	0·0796	0·0012	493·9	7·3						
3·1	482	323	0·67	51	0·000058	<0·01	12·804	0·16780	0·05651	0·00053	0·0781	0·0010	484·9	6·1						
4·1	966	349	0·36	93	0·000052	0·16	12·858	0·14050	0·05803	0·00045	0·0777	0·0009	482·1	5·1						
5·1	171	88	0·51	17	0·000167	0·19	12·925	0·19493	0·05824	0·00133	0·0772	0·0012	479·5	7·0						
6·1	521	211	0·40	51	0·000121	0·09	12·741	0·14835	0·05746	0·00073	0·0784	0·0009	486·6	5·5						
7·1	780	720	0·92	80	0·003511	6·21	12·925	0·14213	0·10705	0·00061	0·0726	0·0008	451·6	4·8*						
8·1	324	192	0·59	33	0·000153	0·27	12·775	0·16457	0·05890	0·00103	0·0781	0·0010	484·6	6·1						
9·1	375	265	0·71	38	0·000457	0·92	12·948	0·21117	0·06416	0·00086	0·0765	0·0013	475·3	7·5						
10·1	222	74	0·33	22	0·000188	0·15	12·607	0·18165	0·05788	0·00073	0·0792	0·0011	491·4	6·8						
11·1	255	77	0·30	24	0·000010	0·43	12·872	0·53765	0·06018	0·00118	0·0774	0·0032	480·3	19·4						
12·1	488	204	0·42	49	—	<0·01	12·475	0·14546	0·05636	0·00088	0·0802	0·0009	497·3	5·6						
13·1	381	248	0·65	42	0·000022	<0·01	12·247	0·42946	0·05485	0·00119	0·0818	0·0029	507·1	17·1*						
14·1	570	366	0·64	60	—	0·22	12·750	0·35769	0·05850	0·00073	0·0783	0·0022	485·7	13·1						
15·1	336	214	0·64	34	0·000249	0·78	13·148	0·17950	0·06306	0·00107	0·0755	0·0010	469·0	6·2						
MSWD = 1·4										Weighted mean		484·2								
<b>3. S-type granite Group</b>																				
Sample TUA-1029 Tuani Cordierite Granite, Sierra de Chepes (31° 08' 00"S; 66° 32' 50"W)																				
1·1	496	311	0·63	74	0·000010	0·02	8·837	0·07377	0·06237	0·00055	0·1118	0·0015	683·1	8·5*						
2·1	739	90	0·12	87	0·000008	0·06	9·706	0·05550	0·06091	0·00058	0·1017	0·0012	624·6	6·9*						
3·1	661	339	0·51	76	0·000085	<0·01	10·984	0·06650	0·05842	0·00070	0·0900	0·0011	555·4	6·2*						
4·1	550	500	0·91	59	0·000042	0·12	12·945	0·10518	0·05769	0·00089	0·0762	0·0010	473·6	5·9						
4·2	433	329	0·76	45	—	0·06	13·248	0·07730	0·05722	0·00065	0·0745	0·0009	463·4	5·2						
5·1	576	44	0·08	102	0·000022	0·04	6·461	0·03411	0·07203	0·00045	0·1529	0·0017	977·9	13·6*						
6·1	512	219	0·43	112	0·000013	0·02	5·745	0·04163	0·07378	0·00045	0·1720	0·0021	1030·4	14·1*						
7·1	411	285	0·69	43	0·000010	0·03	12·739	0·08276	0·05691	0·00055	0·0775	0·0009	481·4	5·5						
7·2	136	94	0·69	15	0·000010	0·05	12·440	0·13124	0·05709	0·00103	0·0794	0·0012	492·5	6·9						
8·1	419	526	1·26	52	0·000010	0·17	12·126	0·08257	0·05811	0·00061	0·0813	0·0010	504·1	5·9*						
9·1	308	117	0·38	30	0·000254	0·36	12·502	0·12940	0·05958	0·00078	0·0788	0·0011	488·7	6·8						
10·1	707	256	0·36	76	—	<0·01	11·380	0·05496	0·05769	0·00039	0·0869	0·0010	536·9	5·7*						
11·1	378	194	0·51	46	0·000016	0·01	10·505	0·07681	0·05944	0·00057	0·0940	0·0012	579·4	6·9*						
12·1	210	166	0·79	22	0·000202	0·28	12·674	0·09617	0·05896	0·00139	0·0777	0·0010	482·6	5·9						
13·1	136	101	0·74	14	0·000302	0·25	12·796	0·36638	0·05871	0·00103	0·0770	0·0023	478·3	14·0						
14·1	344	25	0·07	50	0·000010	0·02	7·746	0·14346	0·06629	0·00153	0·1275	0·0027	810·8	49·2*						
15·1	332	218	0·66	45	0·000114	0·05	9·624	0·07186	0·06090	0·00057	0·1026	0·0013	629·7	7·5*						
16·1	273	117	0·43	30	0·000188	0·15	11·526	0·08954	0·05921	0·00068	0·0856	0·0011	529·4	6·5*						
17·1	148	93	0·63	32	0·000027	0·05	6·121	0·05736	0·07028	0·00074	0·1614	0·0022	925·2	24·7*						
18·1	309	122	0·39	45	0·000083	<0·01	8·473	0·07288	0·06119	0·00070	0·1166	0·0015	711·1	8·9*						
MSWD = 2·7										Weighted mean		478·6								
Sample VMA-1018 Porphyritic monzogranite, Sierra de Mazán, Velasco batholith (28° 43' 31"S; 66° 34' 31"W)																				
1·1	313	30	0·09	21	0·000073	0·12	13·411	0·21241	0·05782	0·00073	0·0745	0·0012	463·1	7·1*						
2·1	191	205	1·07	17	0·000324	0·28	12·948	0·19046	0·05912	0·00157	0·0770	0·0011	478·3	6·8						
3·1	505	41	0·08	36	0·000224	0·08	12·698	0·15407	0·05750	0·00050	0·0787	0·0010	488·3	5·7						
4·1	425	31	0·07	30	0·000199	0·18	12·704	0·15567	0·05830	0·00087	0·0786	0·0010	487·6	5·8						
5·1	508	411	0·81	43	0·000044	0·04	12·941	0·24597	0·05715	0·00077	0·0772	0·0015	479·6	8·8						
6·1	219	156	0·71	18	0·000212	0·41	13·062	0·21666	0·06018	0·00105	0·0762	0·0013	473·6	7·6						
7·1	454	27	0·06	32	0·000084	0·06	12·746	0·15733	0·05735	0·00072	0·0784	0·0010	486·6	5·8						
8·1	285	122	0·43	22	0·000298	<0·02	12·520	0·19901	0·05663	0·00085	0·0799	0·0013	495·5	7·6						
9·1	19	21	1·13	9	0·001382	2·12	2·360	0·08425	0·13494	0·00204	0·4148	0·0148	2236·6	68·0*						
10·1	352	19	0·05	25	0·000271	0·04	12·715	0·18498	0·05713	0·00062	0·0786	0·0012	487·9	6·9						
11·1	697	36	0·05	48	0·000286	0·14	12·793	0·15492	0·05798	0·00051	0·0781	0·0010	484·5	5·7						
12·1	472	33	0·07	32	0·000116	<0·01	13·017	0·17230	0·05674	0·00058	0·0768	0·0010	477·2	6·1						
13·1	331	24	0·07	23	0·000193	0·11	12·840	0·17921	0·05774	0·00089	0·0778	0·0011	482·9	6·5						
14·1	471	35	0·07	33	0·000161	0·11	12·736	0·16001	0·05772	0·00053	0·0784	0·0010	486·7	5·9						
15·1	519	35	0·07	36	-0·000031	0·23	12·884	0·15357	0·05866	0·00077	0·0774	0·0009	480·8	5·5						
16·1	494	39	0·08	34	0·000141	0·08	12·823	0·15218	0·05748	0·00050	0·0779	0·0009	483·7	5·5						
17·1	542	40	0·07	38	0·000025	0·16	12·759	0·14997	0·05811	0·00057	0·0783	0·0009	485·7	5·5						
MSWD = 0·61										Weighted mean		1·6								
Sample CAP-1021 Cordierite monzogranite, Sierra de Capillitas (27° 27' 03"S; 66° 23' 30"W)																				
1·1	289	185	0·64	29	0·000106	0·08	13·210	0·17139	0·05710	0·00067	0·0756	0·0010	470·0	5·9						
2·1	217	116	0·53	21	0·000077	0·02	13·119	0·19492	0·05662	0·00084	0·0762	0·0011	473·5	6·8						
3·1	390	17	0·04	34	—	0·18	12·881	0·16386	0·05791	0·00068	0·0775	0·0010	481·1	5·9						
4·1	290	158	0·55	28	0·000010	0·13	13·364	0·16168	0·05754	0·00094	0·0747	0·0009	464·6	5·5						
5·1	586	93	0·16	52	0·000098	<0·01	13·322	0·15741	0·05587	0·00059	0·0751	0·0009	466·9	5·3						
5·2	129	55	0·42																	

Table 2 (continued)

Grain spot	U ppm	Th ppm	Th/U	Pb* ppm	$^{204}\text{Pb}/^{206}\text{Pb}$	$f_{206}$ %	Measured ratios			Radiogenic		Age (Ma)							
							$^{238}\text{U}/^{206}\text{Pb}$	s.d.	$^{207}\text{Pb}/^{206}\text{Pb}$	s.d.	$^{206}\text{Pb}/^{238}\text{U}$	s.d.	$^{206}\text{Pb}/^{238}\text{U}$	s.d.					
<b>3. S-type granite Group (continued)</b>																			
Sample VEL-1026, Two-mica porphyritic monzogranite, La Puerta, Velasco Batholith ( $29^{\circ} 20' 49''\text{S}$ ; $67^{\circ} 15' 08''\text{W}$ )																			
<b>SHRIMP II</b>																			
1-1	446	45	0.10	40	0.000162	0.02	12.926	0.15706	0.05689	0.00095	0.0773	0.0009	480.3	5.7					
2-1	365	35	0.10	32	0.000057	0.19	12.991	0.19200	0.05826	0.00094	0.0768	0.0011	477.2	6.8					
3-1	399	60	0.15	36	0.000016	0.06	13.026	0.17841	0.05719	0.00068	0.0767	0.0011	476.5	6.3					
4-1	327	104	0.32	30	0.000145	0.20	13.242	0.18148	0.05836	0.00070	0.0754	0.0010	468.4	6.2					
5-1	397	44	0.11	35	0.000005	0.08	12.978	0.15570	0.05735	0.00080	0.0770	0.0009	478.1	5.6					
6-1	488	54	0.11	44	0.000010	<0.01	12.789	0.16495	0.05637	0.00087	0.0782	0.0010	485.5	6.1					
7-1	690	47	0.07	61	0.000052	0.03	12.949	0.15308	0.05693	0.00057	0.0772	0.0009	479.4	5.5					
8-1	518	120	0.23	49	—	0.13	12.730	0.15701	0.05777	0.00054	0.0785	0.0010	486.9	5.8					
9-1	323	34	0.11	29	0.000010	0.01	12.865	0.16848	0.05677	0.00068	0.0777	0.0010	482.5	6.1					
10-1	612	59	0.10	54	0.000052	0.13	12.976	0.14373	0.05771	0.00089	0.0770	0.0009	478.0	5.1					
11-1	378	33	0.09	34	—	<0.01	12.868	0.16235	0.05429	0.00076	0.0780	0.0010	483.9	5.9					
12-1	591	92	0.16	53	—	<0.01	13.093	0.16244	0.05666	0.00055	0.0764	0.0010	474.5	5.7					
13-1	683	86	0.13	61	0.000111	0.11	12.926	0.14772	0.05759	0.00071	0.0773	0.0009	479.9	5.3					
13-2	694	85	0.12	63	0.000093	0.10	12.806	0.15105	0.05752	0.00053	0.0780	0.0009	484.2	5.5					
14-1	296	103	0.35	28	0.000075	0.13	13.147	0.17425	0.05778	0.00094	0.0760	0.0010	472.0	6.1					
15-1	379	35	0.09	34	0.000220	<0.01	12.978	0.16152	0.05587	0.00077	0.0771	0.0010	479.0	5.8					
<b>SHRIMP I</b>																			
2-3	425	39	0.09	25	0.000010	<0.01	12.473	0.19140	0.05576	0.00079	0.0803	0.0012	497.7	7.4					
3-2	689	98	0.14	42	0.000010	0.06	12.265	0.17387	0.05717	0.00079	0.0815	0.0012	505.0	6.9*					
10-2	423	40	0.09	39	0.000046	0.23	13.029	0.18658	0.05857	0.00098	0.0766	0.0011	475.6	6.6					
11-2	256	17	0.07	25	0.000063	<0.01	12.171	0.18263	0.05666	0.00093	0.0823	0.0012	509.5	7.4*					
16-1	473	38	0.08	46	0.000064	<0.01	12.462	0.17018	0.05603	0.00092	0.0804	0.0011	498.3	6.6					
16-2	561	20	0.04	52	0.000014	<0.01	12.914	0.19081	0.05604	0.00078	0.0775	0.0012	481.2	6.9					
17-1	323	50	0.16	30	0.000320	0.11	13.034	0.19471	0.05759	0.00090	0.0766	0.0012	476.0	6.9					
17-2	464	26	0.06	27	0.000060	0.07	12.679	0.19828	0.05727	0.00098	0.0788	0.0012	489.0	7.4					
18-1	167	23	0.14	15	—	<0.01	13.325	0.26572	0.05653	0.00189	0.0751	0.0015	466.6	9.0					
19-1	251	213	0.85	30	0.000010	0.03	12.330	0.19223	0.05746	0.00106	0.0811	0.0013	502.6	7.6*					
20-1	255	31	0.12	22	0.000236	0.19	13.812	0.25673	0.05820	0.00143	0.0723	0.0014	449.8	8.1*					
20-2	420	56	0.13	41	0.000236	<0.01	12.699	0.20740	0.05660	0.00075	0.0788	0.0013	489.0	7.7					
21-1	131	43	0.33	34	0.000077	0.14	5.111	0.12150	0.07834	0.00111	0.1954	0.0047	1150.4	25.1*					
21-2	801	14	0.02	45	0.000069	0.08	12.762	0.16754	0.05737	0.00109	0.0783	0.0010	485.9	6.2					
22-1	252	73	0.29	15	—	<0.01	12.988	0.23251	0.05628	0.00115	0.0770	0.0014	478.4	8.3					
23-1	1023	489	0.48	74	—	<0.01	11.401	0.13694	0.05658	0.00049	0.0879	0.0011	542.9	6.3*					
24-1	762	20	0.03	44	0.000072	<0.01	12.527	0.17979	0.05554	0.00070	0.0799	0.0012	495.8	6.9					
24-2	286	84	0.29	17	0.000154	0.06	13.380	0.22866	0.05718	0.00143	0.0747	0.0013	464.4	7.7					
25-1	365	38	0.10	21	—	<0.01	13.066	0.18941	0.05436	0.00133	0.0768	0.0011	476.7	6.7					
26-1	226	53	0.23	13	0.000010	0.07	13.208	0.29231	0.05730	0.00140	0.0757	0.0017	470.1	10.1					
27-1	223	27	0.12	13	0.000067	<0.01	12.557	0.21864	0.05566	0.00133	0.0797	0.0014	494.6	8.3					
28-1	655	61	0.09	38	0.000045	<0.01	12.747	0.18358	0.05626	0.00066	0.0785	0.0011	487.1	6.8					

MSWD = 1.4

Weighted mean

481.0

1.1

1. Uncertainties given at the one s level; \* data omitted from weighted mean.

2.  $f_{206}$  % denotes the percentage of  $^{206}\text{Pb}$  that is common Pb.3. For ages > 800 Ma, correction for common Pb made using the measured  $^{204}\text{Pb}/^{206}\text{Pb}$  ratio.4. For ages < 800 Ma, correction for common Pb made using the measured  $^{238}\text{U}/^{206}\text{Pb}$  and  $^{207}\text{Pb}/^{206}\text{Pb}$  following Tera & Wasserburg (1972) as outlined in Compston *et al.* (1992).

including the 500 Ma 'event'; the best estimate of the crystallisation age is  $478 \pm 4$  Ma (Fig. 6). The other sample is a typical calc-alkaline granodiorite (SVF-593), which gave a slightly younger age of  $470 \pm 5$  Ma (Table 2). Two samples were investigated from the Sierra de Famatina in northwestern La Rioja (Fig. 1). VCA-1007 is another gabbro, from the Cerro Toro complex. This unit displays hybridisation between the gabbro and granite, the latter having a published Rb-Sr age of  $456 \pm 14$  Ma (Saavedra *et al.* 1992). Apart from one analysis showing minor Pb loss, the SHRIMP data are well constrained and give a precise age of  $468 \pm 3$  Ma (Fig. 6), similar to that for the granodiorite SVF-593. Finally, zircon from the main granitic unit of the Sierra de Famatina, the Nuñorco granite, was analysed (sample MIR-1014). This cataastically-altered sample of coarse porphyritic biotite-hornblende granite gave a SHRIMP age of  $484 \pm 5$  Ma (Fig. 6). This is considerably older than previously published K-Ar cooling ages (up to 449 Ma, Gonzalez *et al.* 1985) and a lower U-Pb intercept for rather discordant zircon fractions (459 Ma, Loske & Miller 1996). We consider that an Early Ordovician age similar to those of the I-type granitoids of southern La Rioja is now established for this

unit. The total age range determined for these rocks by U-Pb zircon dating is 468–486 Ma, all but two falling in the more limited range of 477–486 Ma.

### 3.3. S-type granites

Pankhurst *et al.* (1998) identified sporadic outcrops of xenolithic S-type cordierite granite (Tuaní Granite) in the roof zone of the Chepes Granodiorite of southern La Rioja. The typical optical and cathodo-luminescence characteristics of zircons in a sample of this rock (TUA-1029) are depicted in Figure 4. A wide variety of rounded, prismatic, acicular and sub-rounded elongate forms are present, suggesting a complex provenance. In the cathodo-luminescence image, it is clear that many of the grains have overgrowths on older zoned cores, and that these have wide-ranging ages. The crystallisation age of this rock could only be determined from the zoned tip overgrowths of externally well-formed needles. The full data set is shown in Figure 7. A resolved group of data points for magmatic overgrowths gives an age of  $479 \pm 10$  Ma, fully consistent with the age of the I-type magmatism in this area. Scattered inheritance up to 1030 Ma is demonstrated by the remaining data, which are notably discordant (i.e. the points fall directly

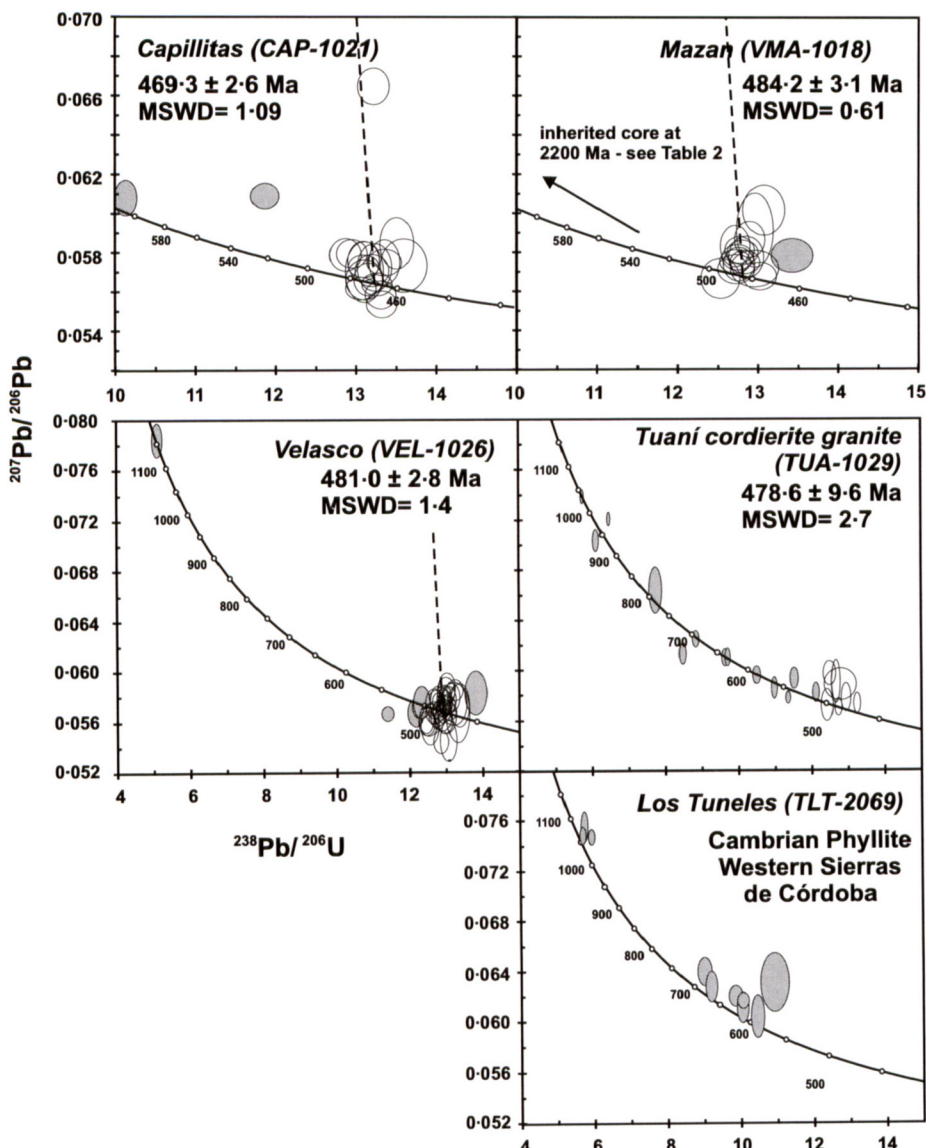


Figure 7 Tera-Wasserburg diagrams for S-type Famatinian granitoids; comments as for Figure 5.

on the Concordia curve, indicating that they are almost certainly individually significant). The pattern of inheritance is considered further in section 4.

The remaining S-type granites investigated are from the great batholiths of northern La Rioja—Capillitas, Mazán and Velasco (Fig. 1). For the first two, apparent magmatic overgrowths were targeted in order to determine the age of crystallization. This was relatively straightforward for sample VMA-1018, where new zircon seemed to dominate the population; a deliberately chosen remnant core gave an age of 2,200 Ma (well off-scale in Fig. 7), but the remainder plot close to 480 Ma. Ignoring one analysis as having suffered some Pb-loss, an age of  $484 \pm 3$  Ma was calculated. Inheritance at 520 Ma and 600 Ma was clearly apparent in CAP-1021, but again the magmatic event was clearly distinguished at  $469 \pm 3$  Ma. In the sample of the porphyritic facies of the Velasco batholith, VEL-1026, an attempt to date inherited cores in addition to the magmatic zircon was not fruitful. Once again there is evidence of zircon growth at 500 Ma (see also Fig. 4), but a crystallisation age of  $481 \pm 3$  Ma was obtained. It is

notable that this sample from the southwestern part of the batholith, with an ASI index lower than 1.2, gives an age indistinguishable from that of the cordierite-bearing VMA-1018 of the northeastern area, suggesting the bulk of the Velasco batholith was emplaced in a short period of time.

On the basis of these few samples it seems that these major S-type batholiths are not entirely, nor even largely, formed of granites with the high degree of zircon inheritance shown by the Tuaní (Chepes) cordierite granite. This difference is also reflected in the Sr–Nd isotopic relationships, suggesting that a process other than simple upper crustal melting generated these granites.

#### 4. Origin of the Famatinian granites

##### 4.1. Isotopic relationships

A notable feature of the Famatinian event is that the abundant amphibole-bearing, noritic and troctolite gabbros, with less than 50% SiO<sub>2</sub>, share the same elevated initial  $^{87}\text{Sr}/^{86}\text{Sr}$  ratios

(0.706–0.710) as the intermediate and acidic I-type rocks (Pankhurst *et al.* 1998). The new data show that there is some overall composition-related variation in initial  $^{87}\text{Sr}/^{86}\text{Sr}$  ratios and  $\epsilon\text{Nd}_{\text{t}}$  values; the most depleted Valle Fértil gabbro, SVF-591, falls at 0.706 and -2.4, but the gabbros and diorites from southern La Rioja form a particularly tight group in the Sr–Nd diagram at 0.708–0.710 and -5 to -6 (Fig. 8), indistinguishable from the associated granodiorites and monzogranites. This rules out mixing between isotopically juvenile asthenospheric mantle and evolved crustal end members, such as that invoked to explain compositional variation among comparable metaluminous and peraluminous granodiorites in the Iberian Massif (Castro *et al.* 1999). The isotopic signature of the Famatinian I-type granitoids is at the lower- $^{87}\text{Sr}/^{86}\text{Sr}$  end of the field of Pampean orthogneisses and must reflect a source in an isotopically evolved region such as the middle or lower crust, or lithospheric mantle. Depleted mantle model ages ( $T_{\text{DM}}$ ) for the bulk of the Ordovician igneous rocks, both I- and S-types, are in the interval 1500–1700 Ma, indicating derivation from Palaeo- to Mesoproterozoic sources (Pankhurst *et al.* 1998). We propose melting of a Proterozoic crust-mantle section, including the underlying subcontinental mantle, to produce the most basic rocks. The only exceptions are two of the small TTG plutons (San Agustín and La Playa), which appear to have a source in isotopically primitive (?asthenospheric) mantle (Fig. 8). A primitive source with initial  $^{87}\text{Sr}/^{86}\text{Sr} = 0.7032$ –0.7034 has been also inferred for the Ordovician trondhjemites of NW Argentina (Lork *et al.* 1991).

The S-type granites have higher initial  $^{87}\text{Sr}/^{86}\text{Sr}$  ratios and lower  $\epsilon\text{Nd}_{\text{t}}$  values than the I-types (Fig. 8) and fall at the evolved end of the field of Pampean gneisses or in that of the regional Pampean metasediments. The minor Tuaní granites from the Sierras de La Rioja have Sr and Nd characteristics very close to those of the adjacent low-grade metapelites.

This locally restricted granite type generally contains numerous xenoliths of metasedimentary type. In addition, the cordierite-bearing granite of this facies (TUA-1029) has a fully developed pattern of zircon inheritance that is comparable to that of the low-grade Cambrian metasediments (TLT-2069), with scattered Neoproterozoic provenance back to 9050–1150 Ma (Figs 4, 7). Thus we suggest that granites of this group were derived by local anatexis of the envelope of the I-type granodiorites. Such an origin does not apply to the major batholiths with abundant S-type granite facies farther N. The single sample of the Capillitas granite has evolved initial Sr- and Nd-isotope compositions comparable to that of the higher grade Pampean gneisses, which might represent a deeper, middle crustal source region. The Velasco samples have compositions that merge into the I-type field. At this stage we have insufficient zircon inheritance data on the larger bodies of Capillitas and Velasco, but they clearly contain some older zircon (Fig. 7) and crustal melts must have contributed very significantly in their petrogenesis, perhaps through hybridisation with the I-type granodioritic melts.

#### 4.2. Trace element modelling: TTG and I-type granites

There is no direct exposure of deep crust within the Sierras Pampeanas, but some evidence for its composition comes from xenoliths in younger igneous rocks. Lucassen *et al.* (1999) investigated granulite xenoliths from Cretaceous basanite intrusions that are considered to be deep crustal samples of the widespread Early Palaeozoic supracrustal sequences of the northern Sierras Pampeanas. Mafic granulite A-112a (Lucassen *et al.* 1999), which equilibrated at 900 °C and 9.5–10.5 kbar, is very similar to the relatively LILE- and light REE-enriched hornblende gabbros of the Sierra de Valle Fértil, such as sample SVF-591 (see Table 1 and Figs 9–11), except that it has a positive  $\epsilon\text{Nd}$  at 480 Ma (Fig. 8). Water-undersaturated partial fusion experiments of compositionally

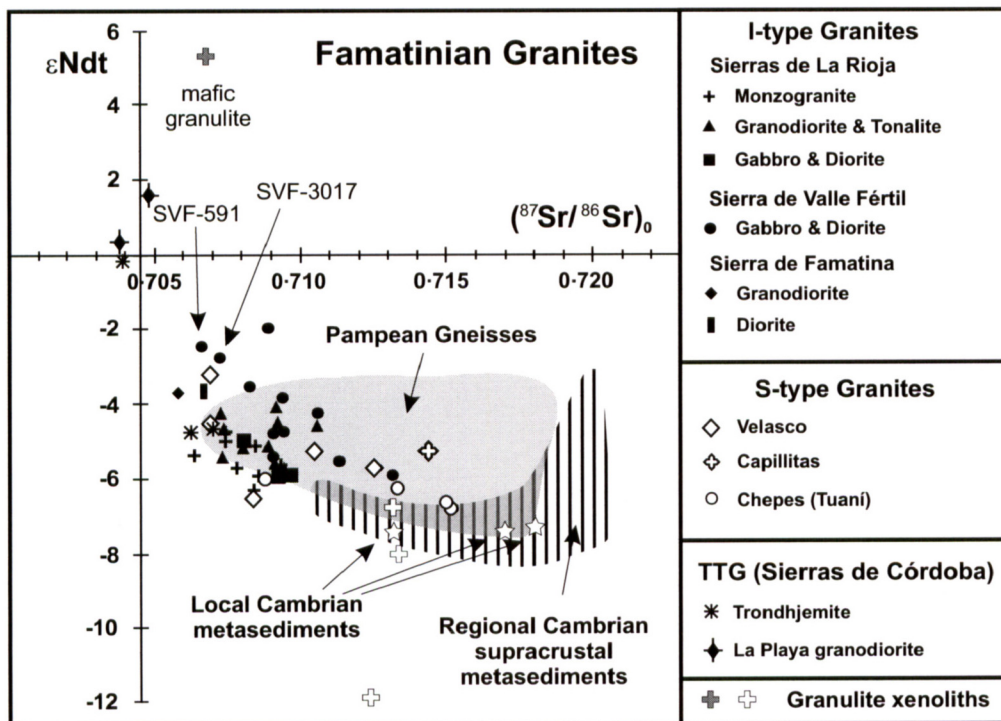


**Figure 8** Initial Sr–Nd isotope composition plot for the granitoids of the Famatinian belt, compared to fields for Early Palaeozoic gneisses and phyllites at 480 Ma—white stars represent samples from the envelope of the Chepes granodiorite and Tuaní granite (Pankhurst *et al.* 1998 and authors' additional unpublished data); key samples and the granulite xenolith data of Lucassen *et al.* 1999 are also indicated.

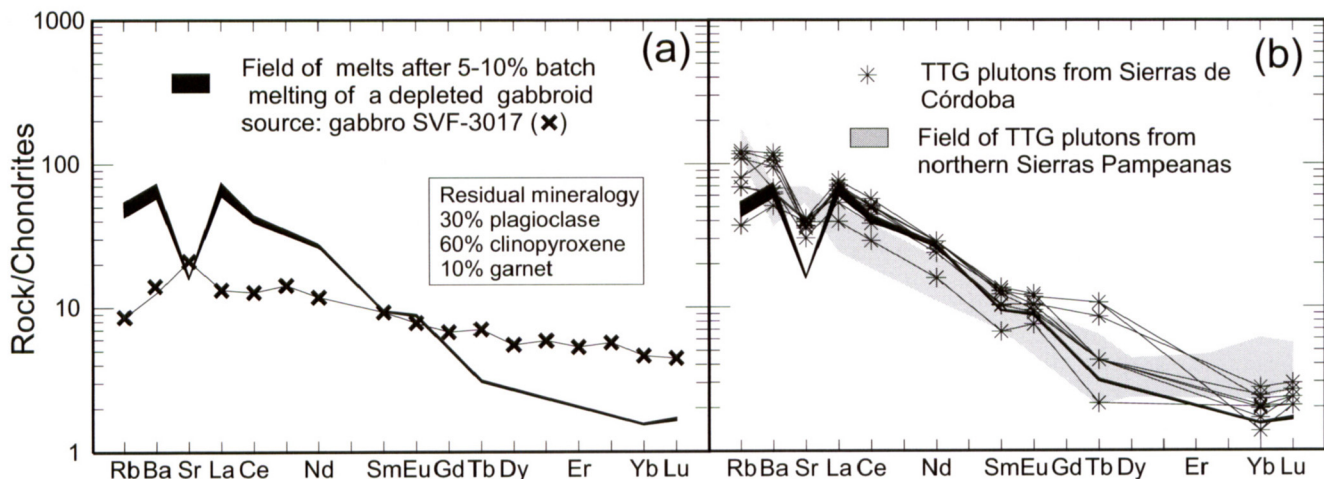


**Figure 9** Trace element diagrams normalised to chondrite (Sun & McDonough 1989) for the Famatinian TTG granitoids: (a) model for TTG plutons; partial melt and residue compositions are obtained from batch modal melting equations (Shaw 1970);  $K_d$  values as follows: REE in plagioclase, opx, cpx, hornblende and garnet (Springer & Seck 1997), except Eu in plagioclase (Fujimaki *et al.* 1984); REE and LILE in K-feldspar (Nash & Crecraft 1985); LILE in plagioclase, opx, cpx and hornblende (Bacon & Druitt 1988); LILE in garnet (Arth 1976); the source rock used is a depleted pyroxene-hornblende gabbro from Sierra de Valle Fértil (SVF-3017, Table 1). (b) Composition of trondhjemite plutons from Sierras de Córdoba (Gúiraldes and La Fronda, Rapela *et al.* 1998); scatter in Tb is probably due to poor precision in INAA determinations; melt field repeated from (a) for comparison. TTG field from northern Sierras Pampeanas (Sierra de Cachi) is based on three samples (Galliski & Miller 1989).

similar basic granulites at 5–15 kbar show that while plagioclase and pyroxene dominate the crystalline residua at 5 kbar, pyroxene–garnet assemblages dominate at 15 kbar (Springer & Seck 1997). The modal composition of experimental residues reported by these authors at 10–12 kbar is very similar to the modal composition of granulite A-112a (30% plagioclase, 60% clinopyroxene, 10% garnet; F. Lucassen, pers. comm.), which is used here in the geochemical modelling of TTG and the intermediate I-type granites. An alternative approach to the modelling is to treat the I-types as probable melts of basaltic underplating, the composition of which might be estimated from the most primitive (LILE-poor) gabbros in the Famatinian Belt itself, which should represent large percentages of melting. Both ‘enriched’ and more incompatible element-depleted opx–cpx–hornblende gabbros, such as samples SVF-591 and SVF-3017, respectively (Table 1), are

of widespread occurrence in the Sierra de Valle Fértil. These samples were also considered as compositionally equivalent to potential sources in the modelling diagrams (Figs 9, 10).

Calculated liquids after 5–10% equilibrium partial melting of the ‘enriched’ gabbroid sources (SVF-591 and A-112a), with the granulitic xenolith modal assemblage as the melting residue, are characterised by high La/Yb ratios, positive or absent Eu anomalies and Sr negative anomalies (Fig. 9a). Although this matches the general characteristics of the Famatinian TTG, La, Ce and especially Rb and Ba are much lower in the latter, suggesting derivation from a mafic source poorer in highly incompatible elements, such as the gabbro SVF-3017 (Fig. 9a). The depleted basaltic source inferred previously for the trondhjemite plutons of the northern Sierras Pampeanas (Galliski *et al.* 1990) is thus confirmed here for the Sierras de Córdoba TTG. The widespread occurrence of

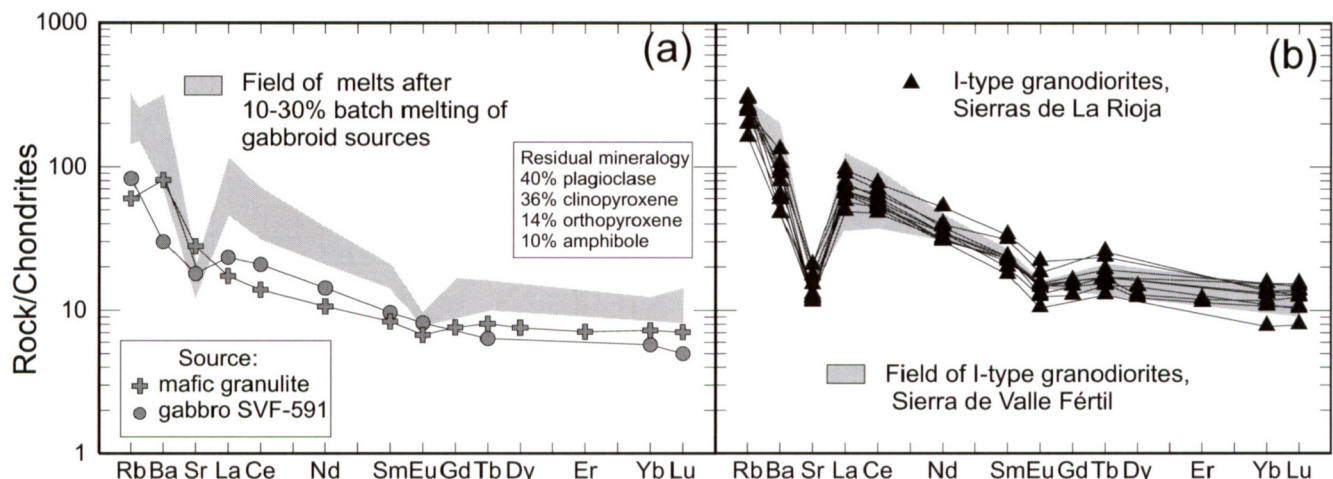


**Figure 10** Trace element diagrams normalised to chondrite (Sun & McDonough 1989) for I-type granitoids of the Famatinian arc: (a) geochemical modelling for I-type granodiorites; partial melting equations and  $K_d$  values as in Figure 9; source rocks are enriched gabbro SVF-591 (Table 1) and mafic granulite xenolith A-112a from the northern Sierras Pampeanas (Lucassen *et al.* 1999); (b) compositions of Sierras de La Rioja hornblende–biotite granodiorites with 60–66% SiO<sub>2</sub> (Sierra de Chepes, Pankhurst *et al.* 1998); the field of hornblende–biotite granodiorites from Sierra de Valle Fértil is based on seven samples.

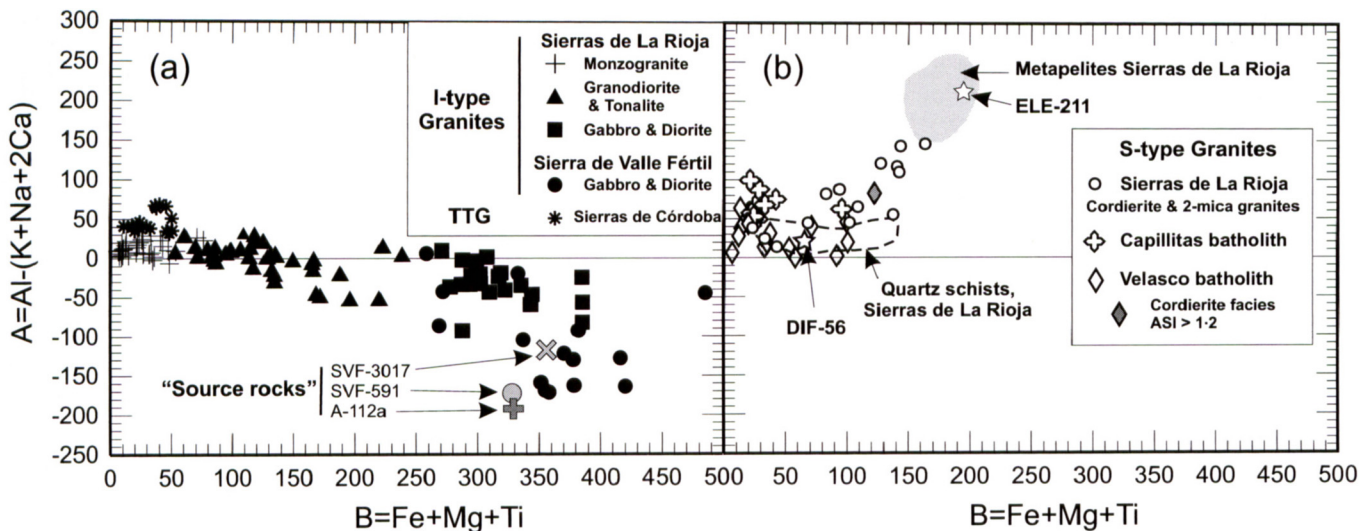


**Figure 11** Multi-cationic plot of Debon & Le Fort (1983), showing major overall element variation in the I-type (a) and S-type (b) suites of the Famatinian belt compared to the inferred source rocks used in the trace element modelling.

trondhjemite plutons of similar age and composition suggests that the residual Early Palaeozoic lower crust inferred by Lucassen *et al.* (1999) extends all along the Pampean mobile belt (Fig. 1).

The granodiorites of the Sierras de La Rioja and Sierra de Valle Fértil, which are the most abundant of the I-type suites, show a fairly uniform major element composition and trace element signature (Fig. 10b). The trace element pattern is completely different from that of the TTG plutons, displaying higher total REE, lower La/Yb ratios and negative Eu anomalies. Our model for these uses the enriched basic protoliths (SVF-591 and A-112a) rather than the LILE-depleted gabbroid. Partial melt compositions with a residual mineralogy of plagioclase, clinopyroxene, orthopyroxene and amphibole in modal proportions equal to average noritic gabbros of Sierra de Valle Fértil are shown in Figure 10a. This modal assemblage is very similar to the melting residua of mafic granulites at 5 kbar and 940 °C, in which garnet is not a stable phase (Springer & Seck 1997). Modelled melts at 10–30% partial melting show an excellent fit with the composition of I-type granodiorites both in LILE and REE (Fig. 10). In the absence of garnet, the most important minerals in the solid residue controlling the composition of melts seem to be amphibole and plagioclase. In the multi-cationic plot of Debon & Lefort (1983), it is clear that the proposed source rocks plot together with the more primitive compositions of gabbro and diorite (Fig. 11). The intermediate and acidic I-type granitoids are progressively more evolved, and plot along a trend typical of I-type suites (Villaseca *et al.* 1998). We see no evidence for fractional crystallisation as the overall control and, since there is a significant variation in isotope compositions, variable partial melting of a totally homogeneous source is not likely to be the sole explanation. Some hybridisation of the more basic (lithospheric mantle) melts with crustal melts seems most probable. However, it is significant that the most primitive end-member that we have identified is already isotopically evolved compared to asthenospheric mantle which, as noted above, only appears to be represented in some of the TTG compositions.

#### 4.3. Trace element modelling: S-type granites

Partial melt modelling of metasedimentary sources is hindered by the fact that several trace elements, especially the REE, reside in accessory minerals whose modal abundances and

behaviour are poorly known. Therefore geochemical modelling of the S-type granites is restricted to Rb, Ba and Sr (Fig. 12). Compared to the trondhjemites and I-type granodiorites, the S-type granites plot in a distinct high-Rb, low-Sr field (Fig. 12b). Potential metasedimentary sources in the upper crust are the pelite–sandstone sequences that form the supracrustal envelope of the Sierras Pampeanas from the Puncoviscana Formation in the N to the Sierras de San Luis in the S (Fig. 1). Higher-grade middle crustal levels may also be involved, as suggested by the isotopic comparison with Pampean gneisses (Fig. 8). Compositions from the Sierras de La Rioja (Pankhurst *et al.* 1998; Pascua 1998) were taken as representative of model source rocks (Fig. 11b, 12a), with a residual mineralogy from the average felsic granulite xenoliths of Lucassen *et al.* (1999). The S-type granites of the Sierra de La Rioja follow a trend of increasing peraluminosity with mafic index which approaches the field of the metapelites (Fig. 11b), a characteristic of highly peraluminous granites with peritectic cordierite (Villaseca *et al.* 1998). The LILE compositions of these S-type granites are well modelled by 10–40% melting of the metasedimentary sources (Fig. 12). A less conspicuous trend towards pelitic compositions is evident in cordierite granites of the Velasco batholith with ASI > 1.2, which are also enriched in Rb and depleted in Sr and Ba compared to S-types from La Rioja (Figs 11b, 12b). However, the Capillitas and Velasco granites with lower ASI values do not show this trend. Extraction of peraluminous melts from metasedimentary sources to form extensive S-type facies such as those found in the Velasco and Capillitas batholiths would imply the retention of even greater volumes of LILE-depleted residua in the middle crust and the top of the lower crust. The Rb contents of felsic granulites plot near the lower boundary of the field of modelled residua, while Sr plots above this field. As Rb decreases and Sr increases in the residue with progressive melting (Fig. 12a), this suggests that the felsic granulites are highly depleted residual sources, probably developed through more than one episode of melt extraction. In any case, it would be reasonable to conclude that, during the Famatinian episode, widespread melting of a whole crustal section including lower crustal granulites and supracrustal sediments generated extensive cumulate norites and LILE-depleted felsic granulites that at present constitute the middle and lower levels of the Andean crust. Crustal anatexis of metasediments is probably the most important process

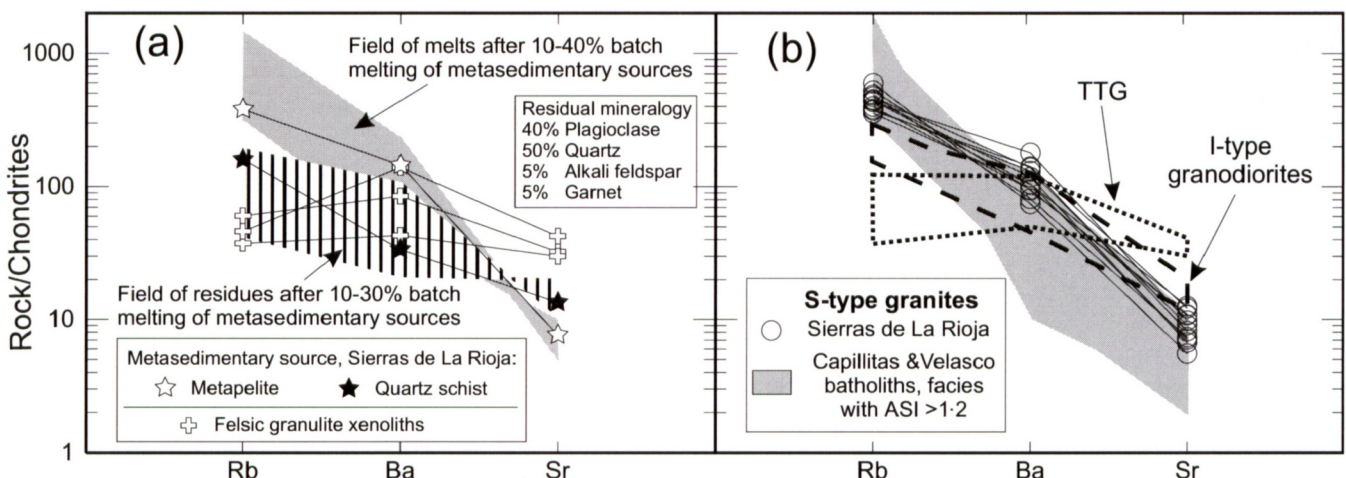


**Figure 12** Rb, Ba, Sr diagrams normalised to chondrite (Sun & McDonough 1989) for S-type granites of the Famatinian arc. (a) Geochemical modelling; partial melting equations and  $K_d$  values (Rb, Ba, Sr) as in Figure 9; source rocks used for modelling are metapelite ELE-211 and quartz schist DIF-56 from Sierras de La Rioja (Pankhurst *et al.* 1998; Pascua 1998); residual mineralogy after 10–40% partial melting of metasedimentary rocks is taken as the average felsic granulite xenolith from northern Sierras Pampeanas (Lucassen *et al.* 1999; F. Lucassen, pers. comm.); (b) compositions of S-type granites from Sierra de Chepes (11 samples) and field of the porphyritic main facies of the Velasco batholith (7 samples)—see Table 1 for selected chemical analyses. TTG and I-type granodiorite fields correspond to samples shown in Figures 9b and 10b.

in the S-type granites of the large batholiths, judging by the other evidence presented in this paper. However, the similarity of the major element compositions of the biotite facies rocks of the Velasco batholith to those of the I-type monzogranites (a trend also visible in Sr–Nd compositions, Figs 8, 12) implies that hybridisation with lower crustal or lithospheric melts also had an important role in their petrogenesis.

## 5. Conclusions

Notwithstanding their distinct geographical distribution, the tonalite–trondhjemite–granodiorite plutons in the E, the I-type calcic metaluminous suites in the W, and the low-Ca peraluminous S-type batholiths in the central sector have been shown to be closely contemporaneous. The U–Pb zircon ages of all units fall in the range 468–499 Ma, which is only increased to 465–504 Ma at the extreme range of estimated errors. Thus emplacement of these Famatinian magmas is entirely constrained to the Late Cambrian–Llanvirn interval, with a main peak in Arenig times (scale of Gradstein & Ogg 1996).

I-type magmatism in the Sierra de Famatina overlaps in age with the main metaluminous units of the Sierras de La Rioja (Pankhurst *et al.* 1998; Sims *et al.* 1998). Our new U–Pb SHRIMP ages on I-type leucogranites suggest that previous mid-to-late Ordovician Rb–Sr whole-rock isochrons obtained on these rocks (Pankhurst *et al.* 1998) are disturbed or reset ages produced by post-emplacement events, such as the penetrative deformation affecting these units. There is now no unequivocal isotopic evidence to indicate that Famatinian magmatism extended into the Late Ordovician. The typical peraluminous granites of the large Capillitas and Velasco batholiths were previously considered to be Silurian–Devonian, largely on the basis of Rb–Sr whole-rock dating (e.g. Rapela *et al.* 1992).

Two plutons of the TTG suite have primitive isotopic characteristics consistent with an asthenospheric mantle source. For the other TTG, and all the I-type and S-types granitoids, by far the greatest expression of Famatinian magmatism, isotopic compositions of Sr and Nd have a consistently crustal signa-

ture, regardless of major element composition. It is proposed that melting in a Proterozoic crust–lithospheric mantle section was the origin of the parent magmas. Geochemical constraints suggest melting at high pressure of a LILE- and LREE-depleted gabbroid source for the TTG. Combined isotopic and geochemical evidence indicates that the source of the I-type tonalite–granodiorites involved partial melting of a rather more enriched lithospheric source at intermediate pressures (garnet absent). There is a clear hiatus in SiO<sub>2</sub> content between these I-type gabbros and the intermediate members of the suite. Our data, including the ages of inherited zircons, suggest that the granodiorite–monzogranite magmas were largely derived by hybridisation between the gabbros and anatexic melts of the crustal components of the section. Restite rich S-type granites from the southern La Rioja have zircon inheritance patterns and Sr and Nd isotopic signatures nearly identical to those of the adjacent low-grade metapelites, indicating derivation by local anatexis of the envelope. This is not true of the major peraluminous batholiths farther N. Although they contain highly peraluminous and isotopically comparable granites, probably also formed by anatexis of metasedimentary sources, the geochemical trends and initial Sr- and Nd-isotope compositions of the Velasco biotite granites merge into the I-type field, suggesting hybridisation with the I-type granodioritic melts. Field and geochemical evidence suggests that the widespread Famatinian magmatism emplaced in the upper crust involved formation of even more extensive depleted residua—cumulate norites and felsic granulites—in the middle and lower crust.

Although similar to models for the middle crust hybrid production of mixed I-type and S-type suites in Australia (Collins 1996) and Spain (Castro *et al.* 1999), our interpretation rejects the involvement of juvenile asthenospheric sources and proposes isotopically mature and coupled crust–lithospheric mantle as the source of both mixing end-members.

## 6. Acknowledgements

We are grateful to the other members of our Sierras Pampeanas research team (J. Saavedra, C. Casquet, E. Baldo, J. Dahlquist

and C. Galindo) for their constant encouragement, intellectual stimulus and assistance in the field. Most of the work was funded by Argentine research grants to CWR (FONCYT PICT98-4189 and CONICET PIP 4148). RJP acknowledges the support of colleagues in British Antarctic Survey.

## 7. References

- Aceñolaza, F. G., Miller, H. and Toselli, A. 1996. Geología del Sistema de Famatina, *Münchener Geologische Hefte*, Reihe A19.
- Arth, J. G. 1976. Behaviour of trace elements during magmatic processes—a summary of theoretical models and their applications. *Journal of Research of the US Geological Survey* **4**, 41–7.
- Bacon, C. R. & Druitt, T. H. 1988. Compositional evolution of the zoned calc-alkaline magma chamber of Mount Mazama, Crater Lake, Oregon. *Contributions to Mineralogy and Petrology* **98**, 224–56.
- Baldo, E. G. A., Murra, J. A., Casquet, C., Galindo, C. & Saavedra, J. 1999. El gáboronítico de la Sierra de Valle Fértil, Sierras Pampeanas, Argentina: condiciones P-T de la etapa coronítica. *Boletín de la Sociedad Española de Mineralogía* **22**-A, 17–18.
- Caffe, P. J. & Baldo, E. G. 1994. El plutón trondjemítico de 'La Fronda', borde occidental de la Sierra de Cuniputo, Córdoba, Argentina. *Actas, 7th Congreso Geológico Chileno, Concepción* **2**, 972–76. Concepción, Chile: Universidad de Concepción, Departamento Ciencias de la Tierra.
- Castro, A., Patiño Douce, A. E., Corretgé, L. G., de la Rosa, J. D., El-Biad, M. & El-Hmidi, H. 1999. Origin of peraluminous granites and granodiorites, Iberian massif, Spain: an experimental test of granite petrogenesis. *Contributions to Mineralogy and Petrology* **135**, 255–76.
- Chappell, B. W. 1996. Compositional variation within granite suites of the Lachlan Fold Belt: its causes and implications for the physical state of granite magma. *Transactions of the Royal Society of Edinburgh: Earth Sciences* **87**, 159–70.
- Chappell, B. W. & White, A. J. R. 1992. I- and S-type granites in the Lachlan Fold Belt. *Transactions of the Royal Society of Edinburgh: Earth Sciences* **83**, 1–26.
- Cisterna, C. E. 1998. La granodiorita de Las Angosturas, Sistema de Famatina, Argentina: caracterización petrográfica y química. *Revista de la Asociación Geológica Argentina* **53**, 57–68.
- Collins, W. J. 1996. Lachlan Fold Belt granitoids: products of three component mixing. *Transactions of the Royal Society of Edinburgh: Earth Sciences* **87**, 171–81.
- Compston, W., Williams, I. S., Kirschvink, J. L., Zhang Zichao & Ma Guoguan 1992. Zircon U-Pb ages from the early Cambrian time-scale. *Journal of the Geological Society of London* **149**, 171–184.
- Dahlquist, J. A. & Baldo, E. G. 1996. Metamorfismo y deformación Famatinianos en la Sierra de Chepes, La Rioja, Argentina. *Actas, XIII Congreso Geológico Argentino y III Congreso de Exploración de Hidrocarburos* **5**, 393–409. Buenos Aires: Asociación Geológica Argentina.
- DeBari, S. M. 1994. Petrogenesis and physical evolution of the Fiambalá gabbronorite, northwestern Argentina: syntectonic magmatism in the deep crust of a continental margin arc. *Journal of Petrology* **35**, 679–713.
- Debon, F. & Le Fort, P. 1983. A chemical-mineralogical classification of common plutonic rocks and associations. *Transactions of the Royal Society of Edinburgh: Earth Sciences* **73**, 135–49.
- Fujimaki, H., Tatsumoto, M. & Aoki, K. 1984. Partition coefficients of Hf, Zr and REE between phenocrysts and groundmasses. Proceedings of the fourteenth lunary and planetary science conference, Part 2. *Journal of Geophysical Research* **89**, Suppl. B662–72.
- Galliski, M. A. & Miller, C. F. 1989. Petrógenesis de las trondjemíticas de Cachi: condicionamientos impuestos por elementos de tierras raras e implicancias tectónicas. *Actas, Reunión sobre Geotransectas de América del Sur*, 58–62. Montevideo, Uruguay: Universidad de la República, Facultad de Agronomía.
- Galliski, M. A., Toselli, A. & Saavedra, J. 1990. Petrology and geochemistry of the Cachi high-alumina trondjemítites, northwestern Argentina. In Kay, S. M. & Rapela, C. W. (eds) *Plutonism from Antarctica to Alaska*, Geological Society of America Special Paper **241**, 91–100.
- Gómez, G. M. & Lira, R. 1998. Geología y aspectos geoquímicos del plutón granítico de La Playa, Sierra de Guasapampa, provincia de Córdoba. *Revista de la Asociación Geológica Argentina* **53**, 291–305.
- Gonzalez, R. L., Omil, M. & Ruiz, D. L. 1985. Observaciones y edades potasio-argón de formaciones de la Sierra de Paimán, Provincia de La Rioja. *Acta Geológica Lilloana* **16**, 281–7.
- Gradstein, F. M. & Ogg, J. 1996. A Phanerozoic time scale. *Episodes* **19**, 3–5.
- Lork, A. & Bahlburg, H. 1993. Precise U-Pb ages of monazites from the Faja Eruptiva de La Puna Oriental, NW Argentina. *Actas, XII Congreso Geológico Argentino y II Congreso de Exploración de Hidrocarburos (Mendoza)* **4**, 1–6. Buenos Aires: Asociación Geológica Argentina.
- Lork, A., Grauert, B., Kramm, U. & Miller, H. 1991. U-Pb investigations of monazite and polyphase zircon: implications for age and petrogenesis of trondjemítites of the southern Cordillera Oriental, NW Argentina. *Actas, 6th Congreso Geológico Chileno (Viña del Mar)*, 398–402. Santiago de Chile: Servicio Nacional de Geología y Minería.
- Loske, W. & Miller, H. 1996. Sistématica U-Pb de circones del granito Núñez-Sañoagasta. In Aceñolaza, F. G., Miller, H. & Toselli, A. (eds) *Geología del Sistema de Famatina*, Münchener Geologische Hefte, Reihe A19, 221–7.
- Lucassen, F., Lewerenz, S., Franz, G., Viramonte, J. & Mezger, K. 1999. Metamorphism, isotopic ages and composition of lower crustal granulite xenoliths from the Cretaceous Salta Rift, Argentina. *Contributions to Mineralogy and Petrology* **134**, 325–41.
- Martino, R., Kraemer, P., Escayola, M., Giambastianai, M. & Arnostio, M. 1995. Transecta de las Sierras Pampeanas de Córdoba a los 32°S. *Revista de la Asociación Geológica Argentina* **50**, 60–77.
- Mirré, J.C. 1976. Descripción geológica de la Hoja 19e, Valle Fértil. Provincias de San Juan y La Rioja. *Boletín de la Secretaría de Estado de Minería, Servicio Geológico Nacional, Argentina* **147**.
- Nash, W. P. & Crecraft, H. R. 1985. Partition coefficients of trace elements in silicic magmas. *Geochimica et Cosmochimica Acta* **49**, 2309–22.
- Pankhurst, R. J., Rapela, C. W., Saavedra, J., Baldo, E., Dahlquist, J., Pascua, I. & Fanning, C. M. 1998. The Famatinian magmatic arc in the central Sierras Pampeanas: an Early-to-Middle Ordovician continental arc on the Gondwana margin. In Pankhurst, R. J. & Rapela, C. W. (eds) *The Proto-Andean Margin of Gondwana, Special Publications of the Geological Society of London* **142**, 343–67.
- Pascua, I. M. 1998. *Las rocas igneas y metamórficas de la Sierra de Los Llanos, La Rioja, Argentina. Evolución famatiniana de un sector del basamento pre-mesozoico andino*. (Ph.D. Thesis, Departamento de Geología, Universidad de Salamanca, Spain).
- Pérez, M. B., Rapela, C. W. & Baldo, E. G. 1996. Geología de los granitoides del sector septentrional de la Sierra Chica de Córdoba. *Actas, XIII Congreso Geológico Argentino y III Congreso de Exploración de Hidrocarburos* **5**, 493–506. Buenos Aires: Asociación Geológica Argentina.
- Rapela, C. W. & Pankhurst, R. J. 1996. Monzonite suites: the innermost Cordilleran plutonism of Patagonia. *Transactions of the Royal Society of Edinburgh: Earth Sciences* **87**, 193–203.
- Rapela, C. W., Toselli, A., Heaman, L. & Saavedra, J. 1990. Granite plutonism of the Sierras Pampeanas: An inner cordilleran Paleozoic arc in the southern Andes. In Kay, S. M. & Rapela, C. W. (eds) *Plutonism from Antarctica to Alaska*, Geological Society of America Special Papers **241**, 77–90.
- Rapela, C. W., Coira, B., Toselli, A. & Saavedra, J. 1992. The Lower Paleozoic magmatism of southwestern Gondwana and the evolution of the Famatinian orogen. *International Geology Review* **34**, 1081–142.
- Rapela, C. W., Pankhurst, R. J., Casquet, C., Baldo, E., Saavedra, J., Galindo, C. and Fanning, C. M. 1998. The Pampean Orogeny of the southern proto-Andes: evidence for Cambrian continental collision in the Sierras de Córdoba. In Pankhurst, R. J. & Rapela, C. W. (eds) *The Proto-Andean Margin of Gondwana, Special Publications of the Geological Society of London* **142**, 181–217.
- Saavedra, J., Pellitero-Pascual, E., Rossi de Toselli, J. N. & Toselli, A. J. 1992. Magmatic evolution of the Cerro Toro granite: a complex Ordovician pluton of northwestern Argentina. *Journal of South American Earth Sciences* **5**, 21–32.
- Saavedra, J., Toselli, A. J., Rossi, J., Pellitero, E. & Durand, F. 1998. The Early Palaeozoic magmatic record of the Famatina system: a review. In Pankhurst, R. J. & Rapela, C. W. (eds) *The Proto-Andean Margin of Gondwana, Special Publications of the Geological Society of London* **142**, 283–95.
- Shaw, D. M. 1970. Trace element fractionation during anatexis. *Geochimica et Cosmochimica Acta* **34**, 237–43.

- Sims, J. P., Ireland, T. R., Camacho, A., Lyons, P., Pieters, P. E., Skirrow, R. G., Stuart-Smith, P. G. & Miró, R. 1998. U-Pb, ThPb and ArAr geochronology in the southern Sierras Pampeanas, Argentina: implications for the Palaeozoic tectonic evolution of the western Gondwana margin. In Pankhurst, R. J. & Rapela, C. W. (eds) *The Proto-Andean Margin of Gondwana, Special Publication of the Geological Society of London* **142**, 181–217.
- Springer, W. & Seck, H. A. 1997. Partial fusion of basic granulites at 5–15 kbar: implications for the origin of TTG magmas. *Contributions to Mineralogy and Petrology* **127**, 30–45.
- Sun, S. & McDonough, W. F. 1989. Chemical and isotopic systematics of oceanic basalts: implications for mantle compositions. In Saunders, A. D. & Norry, M. J. (eds) *Magmatism in the Ocean Basins, Special Publications of the Geological Society of London* **42**, 313–345.
- Villaseca, C., Barbero, L. & Herreros, V. 1998. A re-examination of the typology of peraluminous granite types in intracontinental orogenic belts. *Transactions of the Royal Society of Edinburgh: Earth Sciences* **89**, 113–19.

R. J. PANKHURST, British Antarctic Survey, c/o NERC Isotope Geosciences Laboratory, Keyworth, Nottingham NG12 5GG, U.K.

C. W. RAPELA, Centro de Investigaciones Geológicas, Universidad Nacional de La Plata, 644 Calle No. 1, 1900 La Plata, Argentina

C. M. FANNING, PRIZE, Research School of Earth Sciences, The Australian National University, Mills Road, Canberra, ACT 01201, Australia

MS received 24 February 2000. Accepted for publication 7 June 2000.